



Finite Element Convergence for State-Based Peridynamic Fracture Models

Prashant K. Jha¹  · Robert Lipton¹ 

Received: 29 September 2018 / Revised: 13 February 2019 / Accepted: 31 May 2019 /

Published online: 21 August 2019

© Shanghai University 2019

Abstract

We establish the a priori convergence rate for finite element approximations of a class of nonlocal nonlinear fracture models. We consider state-based peridynamic models where the force at a material point is due to both the strain between two points and the change in volume inside the domain of the nonlocal interaction. The pairwise interactions between points are mediated by a bond potential of multi-well type while multi-point interactions are associated with the volume change mediated by a hydrostatic strain potential. The hydrostatic potential can either be a quadratic function, delivering a linear force–strain relation, or a multi-well type that can be associated with the material degradation and cavitation. We first show the well-posedness of the peridynamic formulation and that peridynamic evolutions exist in the Sobolev space H^2 . We show that the finite element approximations converge to the H^2 solutions uniformly as measured in the mean square norm. For linear continuous finite elements, the convergence rate is shown to be $C_t \Delta t + C_s h^2/\epsilon^2$, where ϵ is the size of the horizon, h is the mesh size, and Δt is the size of the time step. The constants C_t and C_s are independent of Δt and h and may depend on ϵ through the norm of the exact solution. We demonstrate the stability of the semi-discrete approximation. The stability of the fully discrete approximation is shown for the linearized peridynamic force. We present numerical simulations with the dynamic crack propagation that support the theoretical convergence rate.

Keywords Nonlocal fracture models · Peridynamic · State-based peridynamic · Numerical analysis · Finite element approximation

Mathematics Subject Classification 34A34 · 34B10 · 74H55 · 74S05

✉ Robert Lipton
lipton@math.lsu.edu

Prashant K. Jha
prashant.j16o@gmail.com

¹ Department of Mathematics, Louisiana State University, Baton Rouge, LA, USA

1 Introduction

In this work, we study the state-based peridynamic theory and obtain an a priori error bound for the finite element approximation. The peridynamic theory is a reformulation of classical continuum mechanics carried out in the work of Silling in [34, 37]. The strain inside the medium is expressed in terms of displacement differences as opposed to the displacement gradients. Acceleration of a point is now due to the sum of the forces acting on the point from nearby points. The new kinematics bypasses the difficulty incurred by juxtaposing displacement gradients and discontinuities as in the case of classical fracture theories. The nonlocal fracture theory has been applied numerically to model the complex fracture phenomenon in materials; see [1, 3, 11, 15, 17, 19, 27, 35, 36, 38, 40]. Every point interacts with its neighbors inside a ball of fixed radius is called the horizon. The size of the horizon sets the length scale of the nonlocal interaction. When the forces between points are linear and the nonlocal length scale tends to zero, it is seen that peridynamic models converge to the classic model of the linear elasticity; see [2, 14, 32, 36]. The work of [39] provides an analytic framework for analyzing FEM for the linear bond and state-based peridynamics. For nonlinear forces associated with double well potentials, the peridynamic evolution converges in the small horizon limit to an evolution with a sharp evolving fracture set and the evolution is governed by the classic linear elastic wave equation away from the fracture set; see [21, 25, 26]. A recent review of the state of the art can be found in [4] and [9].

In this work, we assume small deformation and work with the linearized bond-strain. Let $D \subset \mathbb{R}^d$, for $d = 2, 3$, be the material domain. For a displacement field $\mathbf{u} : D \times [0, T] \rightarrow \mathbb{R}^d$, the bond-strain between two material points $\mathbf{x}, \mathbf{y} \in D$ is given by

$$S(\mathbf{y}, \mathbf{x}, t; \mathbf{u}) = \frac{\mathbf{u}(\mathbf{y}, t) - \mathbf{u}(\mathbf{x}, t)}{|\mathbf{y} - \mathbf{x}|} \cdot \frac{\mathbf{y} - \mathbf{x}}{|\mathbf{y} - \mathbf{x}|}. \quad (1)$$

Let $\epsilon > 0$ be the size of the horizon and $H_\epsilon(\mathbf{x}) = \{\mathbf{y} \in \mathbb{R}^d : |\mathbf{y} - \mathbf{x}| < \epsilon\}$ be the neighborhood of a material point \mathbf{x} . For pairwise interaction, we assume the following form of pairwise interaction potential:

$$\mathcal{W}^\epsilon(S(\mathbf{y}, \mathbf{x}, t; \mathbf{u})) = \frac{J^\epsilon(|\mathbf{y} - \mathbf{x}|)}{\epsilon |\mathbf{y} - \mathbf{x}|} f(\sqrt{|\mathbf{y} - \mathbf{x}|} S(\mathbf{y}, \mathbf{x}, t; \mathbf{u})), \quad (2)$$

where $J^\epsilon(|\mathbf{y} - \mathbf{x}|)$ is the influence function. We assume $J^\epsilon(|\mathbf{y} - \mathbf{x}|) = J(|\mathbf{y} - \mathbf{x}|/\epsilon)$ where $0 \leq J(r) \leq M$ for $r < 1$ and $J(r) = 0$ for $r \geq 1$. The potential f , see Fig. 1a, is assumed to be convex for small strains and becomes concave for larger strains. In the widely used prototypical micro-elastic brittle (PMB) peridynamic material, the strain vs force profile is linear up to some critical strain S_c and is zero for any strain above S_c . In contrast, the peridynamic force given by $\partial_S \mathcal{W}^\epsilon$ is linear near zero strain and as the strain gets larger and reaches the critical strain, S_c^+ (S_c^-) for positive (negative) strain, the bond starts to soften, see Fig. 1b. For a given potential function f , the critical strain is given by $S_c^+ = \frac{r^+}{\sqrt{|\mathbf{y}-\mathbf{x}|}}$ and $S_c^- = \frac{r^-}{\sqrt{|\mathbf{y}-\mathbf{x}|}}$, where $r^+ > 0, r^- < 0$ are the inflection points of the potential function f as shown in Fig. 1a.

The spherical or hydrostatic strain $\theta(\mathbf{x}, t; \mathbf{u})$ at material point is given by

$$\theta(\mathbf{x}, t; \mathbf{u}) = \frac{1}{\epsilon^d \omega_d} \int_{H_\epsilon(\mathbf{x})} J^\epsilon(|\mathbf{y} - \mathbf{x}|) S(\mathbf{y}, \mathbf{x}, t; \mathbf{u}) |\mathbf{y} - \mathbf{x}| \, d\mathbf{y}, \quad (3)$$

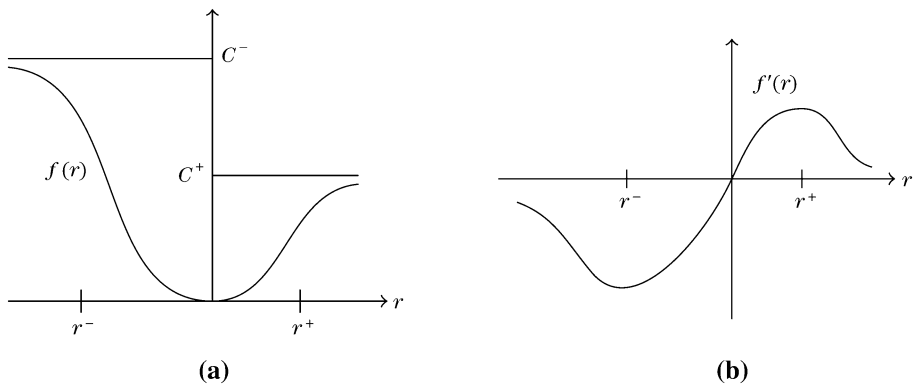


Fig. 1 **a** Potential function $f(r)$ for tensile force. C^+ and C^- are two extreme values of f . **b** Cohesive tensile force

where ω_d is the volume of the unit ball in dimension $d = 2, 3$. The potential for hydrostatic interaction is of the form

$$\mathcal{V}^\epsilon(\theta(\mathbf{x}, t; \mathbf{u})) = \frac{g(\theta(\mathbf{x}, t; \mathbf{u}))}{\epsilon^2}, \quad (4)$$

where g is the potential function associated with the hydrostatic strain. Here g can be of two types: (i) a quadratic function with only one well at zero strain, and (ii) a convex–concave function with a wells at the origin and at $\pm\infty$; see Fig. 2a. If g is assumed to be quadratic, then the force due to the spherical strain is linear. If g is a multi-well potential, the material softens as the hydrostatic strains exceed the critical value. For the convex–concave type g , the critical values are $0 < \theta_c^+ < \theta_c^- < 0$ beyond which the force begins to soften is related to the inflection point r_*^+ and r_*^- of g as follows:

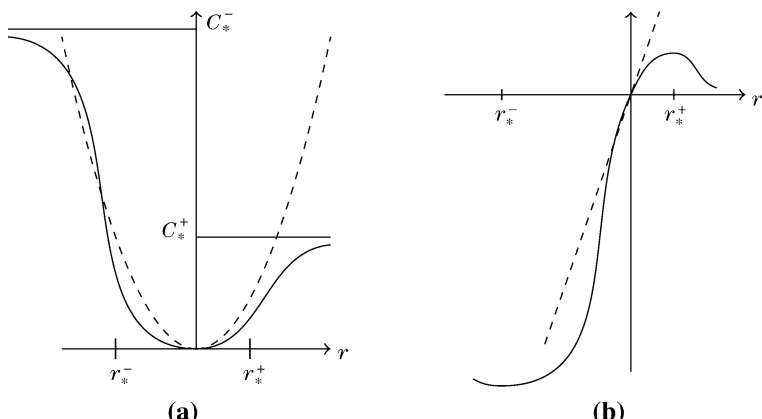


Fig. 2 **a** Two types of potential function $g(r)$ for hydrostatic force. Dashed line corresponds to the quadratic potential $g(r) = \beta r^2/2$. Solid line corresponds to the convex–concave type potential $g(r)$. For the convex–concave type potential, there are two special points r_*^- and r_*^+ at which material points start to soften. C_*^+ and C_*^- are two extreme values. **b** Hydrostatic forces

$$\theta_c^+ = r_*^+, \quad \theta_c^- = r_*^-. \quad (5)$$

The critical compressive hydrostatic strain where the force begins to soften for negative hydrostatic strain is chosen much larger in magnitude than θ_c^+ , i.e., $\theta_c^+ \ll |\theta_c^-|$.

The finite element approximation has been applied to the peridynamic fracture; however, there remains a paucity of literature addressing the rigorous a priori convergence rate of the finite element approximation to peridynamic problems in the presence of material failure. This aspect provides the motivation for the present work. In this paper, we first prove the existence of peridynamic evolutions taking values in $H^2(D; \mathbb{R}^d) \cap H_0^1(D; \mathbb{R}^d)$ that are twice differentiable in time; see Theorem 2. We note that as these evolutions will become more fracture like as the region of the nonlocal interaction decreases. These evolutions can be thought of as inner approximations to fracture evolutions. On passing to subsequences it is possible to show that the $H^2(D; \mathbb{R}^d) \cap H_0^1(D; \mathbb{R}^d)$ evolutions converge in the limit of vanishing non-locality to a limit solution taking values in the space of special functions of bounded deformation SBD. Here the limit evolution has a well-defined Griffith fracture energy bounded by the initial data; see [26] and [23]. We show here that the higher temporal regularity can be established if the body force changes smoothly in time. Motivated by these considerations, we develop finite element error estimates for solutions that take values in $H^2(D; \mathbb{R}^d) \cap H_0^1(D; \mathbb{R}^d)$ and for a bounded time interval.

In this paper, we obtain an a priori L^2 error bound for the finite element approximation of the displacement and velocity using a central in time discretization. Due to the nonlinear nature of the problem, we get a convergence rate using the Lax–Richtmyer stability together with the consistency. Both the stability and consistency are shown to follow from the Lipschitz continuity of the peridynamic force in $L^2(D; \mathbb{R}^d)$; see Sects. 4.2.1 and 4.2.2. The bound on the L^2 error is uniform in time and is given by $C_t \Delta t + C_s h^2/\epsilon^2$, where the constants C_t and C_s are independent of Δt and the mesh size h ; see Theorem 6. A more elaborate discussion of the a priori bound is presented in Sect. 4.2. For the linearized model, we obtain a stability condition on Δt , Theorem 9, that is of the same form as those given for linear local and nonlocal wave equations [18, 24]. We demonstrate the stability for the linearized model noting that for small strains the material behaves like a linear elastic material and that the stability of the linearized model is necessary for the stability of nonlinear model. We believe a more constructive CFL stability condition is possible for the linear case and will pursue this in future work.

Previous work [21] treated spatially Lipschitz continuous solutions and addressed the finite difference approximation and obtained bounds on the L^2 error for the displacement and velocity that are uniform in time and of the form $C_t \Delta t + C_s h/\epsilon^2$, where the constants C_t and C_s are as before. For finite elements, the convergence rate is seen to be slower than for the FEM model introduced here and is of order h/ϵ^2 as opposed to h^2/ϵ^2 . On the other hand, the FEM method increases the computational work due to the inversion of the mass matrix.

We carry out numerical experiments for dynamic crack propagation and obtain convergence rates for Plexiglass that are in line with the theory; see Sect. 5. We also compare the Griffith’s fracture energy with the peridynamic energy of the material softening zone; we show good agreement between the two energies; see Sect. 5.2. Finite difference methods are less expensive than finite element approximations for nonlocal problems; however, the latter offers more control on the accuracy of solution; see [10, 13, 16, 30, 31].

Here the a priori L^2 convergence rates for the FEM given by Theorem 6 include the effects of material degradation through the softening of material properties. The FEM

simulations presented in this paper show that the material develops localized softening zones (region where bonds exceed the critical tensile strain) as it deforms. This is in contrast to linear peridynamic models which are incapable of developing softening zones. For nonlinear peridynamic models with material failure, the localization of zones of softening and damage is the hallmark of the peridynamic modeling [15, 19, 34, 37]. One notes that the a priori error involves ϵ in the denominator and in many cases ϵ is chosen small. However, typical dynamic fracture experiments last only hundreds of microseconds and the a priori error is controlled by the product of simulation time multiplied by h^2/ϵ^2 . So for material properties characteristic of Plexiglass and ϵ of size 4 mm, the a priori estimates predict a relative error of $\frac{1}{10}$ for simulations lasting around 100 μ s. We point out that the a priori error estimates assume the appearance of nonlinearity anywhere in the computational domain. On the other hand, the numerical simulation and independent theoretical estimates show that the nonlinearity concentrates along “fat” cracks of finite length and width equal to ϵ ; see [25, 26]. Moreover, the remainder of the computational domain is seen to behave linearly and to leading order can be modeled as a linear elastic material up to an error proportional to ϵ ; see [Proposition 6, [22]]. Future work will use these observations to focus on the adaptive implementation and a posteriori estimates. A posteriori convergence for FEM models of peridynamics with material degradation can be seen in the work [7, 31, 33]. For other nonlinear and nonlocal models, the adaptive mesh refinement within FE framework for nonlocal models has been explored in [13] and convergence of the adaptive FE approximation is rigorously shown. A posteriori error analysis of linear nonlocal models is carried out in [12].

The paper is organized as follows. We introduce the equation of motion in Sect. 2 and present the Lipschitz continuity of the force, existence of peridynamic solution, and the higher temporal regularity necessary for the finite element error analysis. In Sect. 3, we consider the finite element discretization. We prove the stability of a semi-discrete approximation in Sect. 3.1. In Sect. 4, we analyze the fully discrete approximation and obtain an a priori bound on errors. The stability of the fully discrete approximation linearized peridynamic force is shown in Sect. 4.3. We present our numerical experiments in Sect. 5. Proofs of the Lipschitz bound on the peridynamic force and higher temporal regularity of solutions is provided in Sect. 6. In Sect. 7, we present our conclusions.

We conclude the introduction by listing the notation used throughout the paper. We denote material domain as D , where $D \subset \mathbb{R}^d$ for $d = 2, 3$. Points and vectors in \mathbb{R}^d are denoted as bold letters. Some of the key notations are as follows:

$[0, T]$	Time domain
ϵ	Size of horizon
ρ	Density
$H_\epsilon(\mathbf{x})$	Horizon of $\mathbf{x} \in D$, a ball of radius ϵ centered at \mathbf{x}
ω_d	Volume of unit ball in dimension $d = 2, 3$
$\omega(\mathbf{x}) \in [0, 1]$	Boundary function defined on D taking value 1 in the interior and smoothly decaying to 0 as \mathbf{x} approaches ∂D
\mathbf{u}	Displacement field defined over $D \times [0, T]$. We may also use notation \mathbf{u} to denote field defined over just D
$\mathbf{u}_0, \mathbf{v}_0$	Initial condition on displacement
\mathbf{b}	Body force defined over $D \times [0, T]$
\mathbf{e}_{y-x}	The unit vector pointing from a point y to the point x

$S = S(\mathbf{y}, \mathbf{x}, t; \mathbf{u})$	Bond strain $S = \frac{u(\mathbf{y}, t) - u(\mathbf{x}, t)}{ \mathbf{y} - \mathbf{x} } \cdot \mathbf{e}_{\mathbf{y} - \mathbf{x}}$. We may also use $S(\mathbf{y}, \mathbf{x}; \mathbf{u})$ if \mathbf{u} is a field defined over just D
$\theta = \theta(\mathbf{x}, t; \mathbf{u})$	Spherical or hydrostatic strain. We may also use $\theta(\mathbf{x}; \mathbf{u})$ if \mathbf{u} is a field defined over just D
S_c^+, S_c^-	Critical bond strain
θ_c^+, θ_c^-	Critical hydrostatic strain
$J^\epsilon(r) = J(r/\epsilon)$	Influence function where J is integrable with $J(r) = 0$ for $r \geq 1$ and $0 \leq J(r) \leq M$ for $r < 1$
\bar{J}_a	Moment of function J over $H_1(\mathbf{0})$ with weight $1/(\omega_d \xi ^\alpha)$
f, g	Potential functions for pairwise and state-based interaction
$\mathcal{W}^\epsilon, \mathcal{V}^\epsilon$	Pairwise and state-based potential energy density
$PD^\epsilon(\mathbf{u}(t))$	Total peridynamic potential energy at time t
$\mathcal{E}^\epsilon(\mathbf{u})(t)$	Total dynamic energy at time t
$\mathcal{L}^\epsilon, \mathcal{L}_T^\epsilon, \mathcal{L}_D^\epsilon$	Total peridynamic force, pairwise peridynamic force, and state-based peridynamic force, respectively
$a^\epsilon(\mathbf{u}, \mathbf{v})$	Nonlinear operator where \mathbf{u}, \mathbf{v} are vector fields over D
$a_D^\epsilon, a_T^\epsilon$	Nonlinear pairwise and state-based operator
$\ \cdot\ , \ \cdot\ _\infty, \ \cdot\ _n$	L^2 norm over D , L^∞ norm over D , and Sobolev H^n norm over D (for $n = 1, 2$), respectively
$h, \Delta t$	Size of mesh and size of time step
\mathcal{T}_h	Triangulation of D given by triangular/tetrahedral elements
\mathcal{I}_h	Continuous piecewise linear interpolation operator on \mathcal{T}_h
W	Space of functions in $H^2(D; \mathbb{R}^d)$ such that trace of function is zero on boundary ∂D , i.e., $W = H^2(D; \mathbb{R}^d) \cap H_0^1(D; \mathbb{R}^d)$
V_h	Space of continuous piecewise linear interpolations on \mathcal{T}_h
ϕ_i	Interpolation function of mesh node i
$r_h(\mathbf{u})$	Finite element projection of \mathbf{u} onto V_h
E^k	Total error in mean square norm at time step k
$\mathbf{u}_h^k, \mathbf{v}_h^k$	Approximate displacement and velocity field at time step k
$\mathbf{u}^k, \mathbf{v}^k$	Exact displacement and velocity field at time step k

2 Equation of Motion, Existence, Uniqueness, and Higher Regularity

We assume D to be an open set with C^1 boundary. To enforce zero displacement boundary conditions at ∂D and to insure a well-posed evolution, we introduce the boundary function $\omega(\mathbf{x})$. This function is introduced as a factor into the potentials \mathcal{W}^ϵ and \mathcal{V}^ϵ . Here the boundary function takes value 1 in the interior of domain and is zero on the boundary. We assume $\sup_x |\nabla \omega(\mathbf{x})| < \infty$ and $\sup_x |\nabla^2 \omega(\mathbf{x})| < \infty$ in our analysis. The hydrostatic strain is modified to include the boundary and is given by

$$\theta(\mathbf{x}, t; \mathbf{u}) = \frac{1}{\epsilon^d \omega_d} \int_{H_\epsilon(\mathbf{x})} \omega(\mathbf{y}) J^\epsilon(|\mathbf{y} - \mathbf{x}|) S(\mathbf{y}, \mathbf{x}, t; \mathbf{u}) |\mathbf{y} - \mathbf{x}| \, d\mathbf{y}. \quad (6)$$

The peridynamic potentials, Eqs. 2 and 4, are modified to see the boundary as follows:

$$\mathcal{W}^\epsilon(S(\mathbf{y}, \mathbf{x}, t; \mathbf{u})) = \omega(\mathbf{x}) \omega(\mathbf{y}) \frac{J^\epsilon(|\mathbf{y} - \mathbf{x}|)}{\epsilon |\mathbf{y} - \mathbf{x}|} f(\sqrt{|\mathbf{y} - \mathbf{x}|} S(\mathbf{y}, \mathbf{x}, t; \mathbf{u})), \quad (7)$$

$$\mathcal{V}^\epsilon(\theta(\mathbf{x}, t; \mathbf{u})) = \omega(\mathbf{x}) \frac{g(\theta(\mathbf{x}, t; \mathbf{u}))}{\epsilon^2}. \quad (8)$$

We assume that the potential function f is at least four times differentiable and satisfies the following regularity condition:

$$C_0^f := \sup_r |f(r)| < \infty, \quad C_i^f := \sup_r |f^{(i)}(r)| < \infty, \quad \forall i = 1, 2, 3, 4. \quad (9)$$

If the potential function g is convex–concave type, then we assume that g satisfies the same regularity condition as f . We denote constants C_i^g , for $i = 0, 1, \dots, 4$, similar to C_i^f above.

The total potential energy at time t is given by

$$\begin{aligned} PD^\epsilon(\mathbf{u}(t)) &= \frac{1}{\epsilon^d \omega_d} \int_D \int_{H_\epsilon(\mathbf{x})} |\mathbf{y} - \mathbf{x}| \mathcal{W}^\epsilon(S(\mathbf{y}, \mathbf{x}, t; \mathbf{u})) \, d\mathbf{y} \, d\mathbf{x} \\ &\quad + \int_D \mathcal{V}^\epsilon(\theta(\mathbf{x}, t; \mathbf{u})) \, d\mathbf{x}, \end{aligned} \quad (10)$$

where potential \mathcal{W}^ϵ and \mathcal{V}^ϵ are described above. The material is assumed to be homogeneous and the density is given by ρ . The applied body force is denoted by $\mathbf{b}(\mathbf{x}, t)$. We define the Lagrangian

$$L(\mathbf{u}, \partial_t \mathbf{u}, t) = \frac{\rho}{2} \|\dot{\mathbf{u}}\|^2 - PD^\epsilon(\mathbf{u}(t)) + \int_D \mathbf{b}(t) \cdot \mathbf{u}(t) \, d\mathbf{x},$$

here $\dot{\mathbf{u}}$ is the velocity given by the time derivative of \mathbf{u} . Applying the principal of least action together with a straight forward calculation (see, for example, [28] for detailed derivation) gives the nonlocal dynamics

$$\rho \ddot{\mathbf{u}}(\mathbf{x}, t) = \mathcal{L}^\epsilon(\mathbf{u})(\mathbf{x}, t) + \mathbf{b}(\mathbf{x}, t) \text{ for } \mathbf{x} \in D, \quad (11)$$

where

$$\mathcal{L}^\epsilon(\mathbf{u})(\mathbf{x}, t) = \mathcal{L}_T^\epsilon(\mathbf{u})(\mathbf{x}, t) + \mathcal{L}_D^\epsilon(\mathbf{u})(\mathbf{x}, t), \quad (12)$$

$\mathcal{L}_T^\epsilon(\mathbf{u})$ is the peridynamic force due to the bond-based interaction and is given by

$$\begin{aligned} \mathcal{L}_T^\epsilon(\mathbf{u})(\mathbf{x}, t) \\ = \frac{2}{\epsilon^d \omega_d} \int_{H_\epsilon(\mathbf{x})} \omega(\mathbf{x}) \omega(\mathbf{y}) \frac{J^\epsilon(|\mathbf{y} - \mathbf{x}|)}{\epsilon |\mathbf{y} - \mathbf{x}|} \partial_S f(\sqrt{|\mathbf{y} - \mathbf{x}|} S(\mathbf{y}, \mathbf{x}, t; \mathbf{u})) \mathbf{e}_{\mathbf{y}-\mathbf{x}} \, d\mathbf{y}, \end{aligned} \quad (13)$$

and $\mathcal{L}_D^\epsilon(\mathbf{u})$ is the peridynamic force due to the state-based interaction and is given by

$$\begin{aligned} \mathcal{L}_D^\epsilon(\mathbf{u})(\mathbf{x}, t) \\ = \frac{1}{\epsilon^d \omega_d} \int_{H_\epsilon(\mathbf{x})} \omega(\mathbf{x}) \omega(\mathbf{y}) \frac{J^\epsilon(|\mathbf{y} - \mathbf{x}|)}{\epsilon^2} [\partial_\theta g(\theta(\mathbf{y}, t; \mathbf{u})) + \partial_\theta g(\theta(\mathbf{x}, t; \mathbf{u}))] \mathbf{e}_{\mathbf{y}-\mathbf{x}} \, d\mathbf{y}. \end{aligned} \quad (14)$$

The dynamics is complemented with the initial data

$$\mathbf{u}(\mathbf{x}, 0) = \mathbf{u}_0(\mathbf{x}), \quad \partial_t \mathbf{u}(\mathbf{x}, 0) = \mathbf{v}_0(\mathbf{x}). \quad (15)$$

We prescribe the zero Dirichlet boundary condition on the boundary ∂D

$$\mathbf{u}(\mathbf{x}) = \mathbf{0}, \quad \forall \mathbf{x} \in \partial D. \quad (16)$$

We extend the zero boundary condition outside D to whole \mathbb{R}^d . In our analysis, we will assume the mass density $\rho = 1$ without loss of generality.

2.1 Existence of Solutions and Higher Regularity in Time

We recall that the space $H_0^n(D; \mathbb{R}^d)$ is the closure in the H^n norm of the functions that are infinitely differentiable with compact support in D . For suitable initial conditions and body force, we show that solutions exist in

$$W = H^2(D; \mathbb{R}^d) \cap H_0^1(D; \mathbb{R}^d) = \{v \in H^2(D; \mathbb{R}^d) : \gamma v = 0 \text{ on } \partial D\}, \quad (17)$$

where γ is the trace of the function v on the boundary of D . We will assume that $\mathbf{u} \in W$ is extended by zero outside D . We first exhibit the Lipschitz continuity property and boundedness of the peridynamic force for displacements in W . We will then apply [Theorem 3.2, [20]] to conclude the existence of unique solutions.

We note the following Sobolev embedding properties of $H^2(D; \mathbb{R}^d)$ when D is a C^1 domain.

- From Theorem 2.72 of [8], there exists a constant C_{e_1} independent of $\mathbf{u} \in H^2(D; \mathbb{R}^d)$ such that

$$\|\mathbf{u}\|_\infty \leq C_{e_1} \|\mathbf{u}\|_2. \quad (18)$$

- Further application of standard embedding theorems (e.g., Theorem 2.72 of [8]) shows there exists a constant C_{e_2} independent of \mathbf{u} such that

$$\|\nabla \mathbf{u}\|_{L^q(D; \mathbb{R}^{d \times d})} \leq C_{e_2} \|\nabla \mathbf{u}\|_1 \leq C_{e_2} \|\mathbf{u}\|_2, \quad (19)$$

for any q such that $2 \leq q < \infty$ when $d = 2$ and $2 \leq q \leq 6$ when $d = 3$.

We have the following result which shows the Lipschitz continuity property of a peridynamic force \mathcal{L}^ϵ .

Theorem 1 (Lipschitz continuity of peridynamic force) *Let f be a convex–concave function satisfying $C_i^f < \infty$ for $i = 0, \dots, 4$ and let g either be a quadratic function, or g be a convex–concave function with $C_i^g < \infty$ for $i = 0, \dots, 4$. Also, let the boundary function $\omega : D \rightarrow [0, 1]$ be such that $\sup_{x \in D} |\nabla \omega(x)| < \infty$ and $\sup_{x \in D} |\nabla^2 \omega(x)| < \infty$. Then, for any $\mathbf{u}, \mathbf{v} \in W$, we have*

$$\|\mathcal{L}^\epsilon(\mathbf{u}) - \mathcal{L}^\epsilon(\mathbf{v})\|_2 \leq \frac{\bar{L}_1(1 + \|\mathbf{u}\|_2 + \|\mathbf{v}\|_2)^2}{\epsilon^3} \|\mathbf{u} - \mathbf{v}\|_2, \quad (20)$$

where constant \bar{L}_1 does not depend on ϵ nor \mathbf{u}, \mathbf{v} . Also, for $\mathbf{u} \in W$, we have

$$\|\mathcal{L}^\epsilon(\mathbf{u})\|_2 \leq \frac{\bar{L}_2(\|\mathbf{u}\|_2 + \|\mathbf{u}\|_2^2)}{\epsilon^{5/2}}, \quad (21)$$

where constant \bar{L}_2 does not depend on ϵ nor \mathbf{u} .

Now let $T > 0$ be any positive number, a straight-forward application of [Theorem 3.2, [20]] gives:

Theorem 2 (Existence and uniqueness of solutions over finite time intervals) *Let f , g , and ω satisfy the hypothesis of Theorem 1. For any initial condition $\mathbf{u}_0, \mathbf{v}_0 \in W$, time interval $I_0 = (-T, T)$, and right-hand side $\mathbf{b}(t)$ continuous in time for $t \in I_0$ such that $\mathbf{b}(t)$ satisfies $\sup_{t \in I_0} \|\mathbf{b}(t)\|_2 < \infty$, there is a unique solution $\mathbf{u}(t) \in C^2(I_0; W)$ of peridynamic Eq. 11. Also, $\mathbf{u}(t)$ and $\dot{\mathbf{u}}(t)$ are Lipschitz continuous in time for $t \in I_0$.*

We can also show higher regularity in time of evolutions under suitable assumptions on the body force:

Theorem 3 (Higher regularity) *Suppose the initial data and righthand side $\mathbf{b}(t)$ satisfy the hypothesis of Theorem 2 and suppose further that $\dot{\mathbf{b}}(t)$ exists and is continuous in time for $t \in I_0$ and $\sup_{t \in I_0} \|\dot{\mathbf{b}}(t)\|_2 < \infty$. Then, $\mathbf{u} \in C^3(I_0; W)$ and*

$$\|\partial_{ttt}^3 \mathbf{u}(\mathbf{x}, t)\|_2 \leq \frac{C \left(1 + \sup_{s \in I_0} \|\mathbf{u}(s)\|_2 \right)^2}{\epsilon^3} \sup_{s \in I_0} \|\partial_t \mathbf{u}(s)\|_2 + \|\dot{\mathbf{b}}(\mathbf{x}, t)\|_2, \quad (22)$$

where C is a positive constant independent of \mathbf{u} .

The proofs of Theorems 1 and 3 are given in Sect. 6. For future reference, we note that for any $\mathbf{u}, \mathbf{v} \in L_0^2(D; \mathbb{R}^d)$, we have

$$\|\mathcal{L}^\epsilon(\mathbf{u}) - \mathcal{L}^\epsilon(\mathbf{v})\| \leq \frac{L}{\epsilon^2} \|\mathbf{u} - \mathbf{v}\|, \quad (23)$$

where constant L is given by

$$L := \begin{cases} 4(C_2^f \bar{J}_1 + C_2^g \bar{J}_0^2) & \text{if } g \text{ is a convex-concave type,} \\ 4(C_2^f \bar{J}_1 + g''(0) \bar{J}_0^2) & \text{if } g \text{ is a quadratic function,} \end{cases} \quad (24)$$

and $\bar{J}^\alpha = (\frac{1}{\omega_d}) \int_{H_1(\mathbf{0})} \frac{J(|\xi|)}{|\xi|^\alpha} d\xi$.

2.2 Weak Form

We multiply Eq. 11 by a test function $\tilde{\mathbf{u}}$ in $H_0^1(D; \mathbb{R}^d)$ and integrate over D to get

$$(\ddot{\mathbf{u}}(t), \tilde{\mathbf{u}}) = (\mathcal{L}^\epsilon(\mathbf{u}(t)), \tilde{\mathbf{u}}) + (\mathbf{b}(t), \tilde{\mathbf{u}}). \quad (25)$$

We have the following integration by parts formula:

Lemma 1 *For any $\mathbf{u}, \mathbf{v} \in L_0^2(D; \mathbb{R}^d)$, we have*

$$(\mathcal{L}^\epsilon(\mathbf{u}), \mathbf{v}) = -a^\epsilon(\mathbf{u}, \mathbf{v}), \quad (26)$$

where

$$a^\epsilon(\mathbf{u}, \mathbf{v}) = a_T^\epsilon(\mathbf{u}, \mathbf{v}) + a_D^\epsilon(\mathbf{u}, \mathbf{v}) \quad (27)$$

and

$$\begin{cases} a_T^\epsilon(\mathbf{u}, \mathbf{v}) = \frac{1}{\epsilon^{d+1} \omega_d} \int_D \int_D \omega(\mathbf{x}) \omega(\mathbf{y}) J^\epsilon(|\mathbf{y} - \mathbf{x}|) \\ \quad \cdot \partial_S f(\sqrt{|\mathbf{y} - \mathbf{x}|} S(\mathbf{y}, \mathbf{x}; \mathbf{u})) S(\mathbf{y}, \mathbf{x}; \mathbf{v}) d\mathbf{y} d\mathbf{x}, \\ a_D^\epsilon(\mathbf{u}, \mathbf{v}) = \frac{1}{\epsilon^2} \int_D \omega(\mathbf{x}) g'(\theta(\mathbf{x}; \mathbf{u})) \theta(\mathbf{x}; \mathbf{v}) d\mathbf{x}. \end{cases} \quad (28)$$

The proof of above lemma is identical to the proof of Lemma 4.2 in [28].

Using the above lemma, the weak form of the peridynamic evolution is given by

$$(\ddot{\mathbf{u}}(t), \ddot{\mathbf{u}}) + a^\epsilon(\mathbf{u}(t), \ddot{\mathbf{u}}) = (\mathbf{b}(t), \ddot{\mathbf{u}}). \quad (29)$$

Total dynamic energy We define the total dynamic energy as follows:

$$\mathcal{E}^\epsilon(\mathbf{u})(t) = \frac{1}{2} \|\dot{\mathbf{u}}(t)\|_{L^2}^2 + PD^\epsilon(\mathbf{u}(t)), \quad (30)$$

where PD^ϵ is defined in Eq. 10. The time derivative of the total energy satisfies

$$\frac{d}{dt} \mathcal{E}^\epsilon(\mathbf{u})(t) = (\ddot{\mathbf{u}}(t), \dot{\mathbf{u}}(t)) + a^\epsilon(\mathbf{u}(t), \dot{\mathbf{u}}(t)). \quad (31)$$

Remark 1 It is readily verified that the peridynamic force and energy are bounded for all functions in $L^2(D; \mathbb{R}^d)$. Here the bound on the force follows from the Lipschitz property of the force in $L^2(D; \mathbb{R}^d)$; see Eq. 23. The peridynamic force is also bounded for functions \mathbf{u} in $H^1(D; \mathbb{R}^d)$. This again follows from the Lipschitz property of the force in $H^1(D; \mathbb{R}^d)$ using arguments established in Sect. 6. The boundedness of the energy $PD^\epsilon(\mathbf{u})$ in both $L^2(D; \mathbb{R}^d)$ and $H^1(D; \mathbb{R}^d)$ follows from the boundedness of the bond potential energy $\mathcal{W}^\epsilon(S(\mathbf{y}, \mathbf{x}, t; \mathbf{u}))$ and $\mathcal{V}^\epsilon(\theta(\mathbf{x}, t; \mathbf{u}))$ used in the definition of $PD^\epsilon(\mathbf{u})$; see Eqs. 7 and 8. More generally, this also shows that $PD^\epsilon(\mathbf{u}) < \infty$ for $\mathbf{u} \in L^1(D; \mathbb{R}^d)$.

We next discuss the spatial and the time discretization of peridynamic equation.

3 Finite Element Approximation

Let V_h be given by linear continuous interpolations over tetrahedral or triangular elements \mathcal{T}_h , where h denotes the size of the finite element mesh. Here we assume the elements are conforming and the finite element mesh is shape regular and $V_h \subset H_0^1(D; \mathbb{R}^d)$.

For a continuous function \mathbf{u} on \bar{D} , $\mathcal{I}_h(\mathbf{u})$ is the continuous piecewise linear interpolant on \mathcal{T}_h . It is given by

$$\mathcal{I}_h(\mathbf{u})|_T = \mathcal{I}_T(\mathbf{u}), \quad \forall T \in \mathcal{T}_h, \quad (32)$$

where $\mathcal{I}_T(\mathbf{u})$ is the local interpolant defined over the finite element T and is given by

$$\mathcal{I}_T(\mathbf{u}) = \sum_{i=1}^n \mathbf{u}(\mathbf{x}_i) \phi_i. \quad (33)$$

Here n is the number of vertices in an element T , \mathbf{x}_i is the position of vertex i , and ϕ_i is the linear interpolant associated to vertex i .

Application of Theorem 4.4.20 and Remark 4.4.27 in [5] gives

$$\|\mathbf{u} - \mathcal{I}_h(\mathbf{u})\| \leq ch^2 \|\mathbf{u}\|_2, \quad \forall \mathbf{u} \in W. \quad (34)$$

Let $\mathbf{r}_h(\mathbf{u})$ denote the projection of $\mathbf{u} \in W$ on V_h . For the L^2 norm it is defined as

$$\|\mathbf{u} - \mathbf{r}_h(\mathbf{u})\| = \inf_{\tilde{\mathbf{u}} \in V_h} \|\mathbf{u} - \tilde{\mathbf{u}}\| \quad (35)$$

and satisfies

$$(\mathbf{r}_h(\mathbf{u}), \tilde{\mathbf{u}}) = (\mathbf{u}, \tilde{\mathbf{u}}), \quad \forall \tilde{\mathbf{u}} \in V_h. \quad (36)$$

Since $\mathcal{I}_h(\mathbf{u}) \in V_h$ and Eq. 34, we see that

$$\|\mathbf{u} - \mathbf{r}_h(\mathbf{u})\| \leq ch^2 \|\mathbf{u}\|_2, \quad \forall \mathbf{u} \in W. \quad (37)$$

3.1 Semi-discrete Approximation

Let $\mathbf{u}_h(t) \in V_h$ be the approximation of $\mathbf{u}(t)$ satisfying following for all $t \in [0, T]$,

$$(\dot{\mathbf{u}}_h, \tilde{\mathbf{u}}) + a^e(\mathbf{u}_h(t), \tilde{\mathbf{u}}) = (\mathbf{b}(t), \tilde{\mathbf{u}}), \quad \forall \tilde{\mathbf{u}} \in V_h. \quad (38)$$

We have the following result:

Theorem 4 (Energy stability of semi-discrete approximation) *The semi-discrete scheme is stable and the energy $\mathcal{E}^e(\mathbf{u}_h)(t)$, defined in Eq. 30, satisfies the following bound:*

$$\mathcal{E}^e(\mathbf{u}_h)(t) \leq \left[\sqrt{\mathcal{E}^e(\mathbf{u}_h)(0)} + \int_0^t \|\mathbf{b}(\tau)\| d\tau \right]^2.$$

We note that while proving the stability of semi-discrete scheme corresponding to non-linear peridynamics, we do not require any assumption on the strain $S(\mathbf{y}, \mathbf{x}, t; \mathbf{u}_h)$. The proof is similar to [Section 6.2, [26]].

Proof Letting $\tilde{\mathbf{u}} = \dot{\mathbf{u}}_h(t)$ in Eq. 38 and noting the identity Eq. 31, we get

$$\frac{d}{dt} \mathcal{E}^e(\mathbf{u}_h)(t) = (\mathbf{b}(t), \dot{\mathbf{u}}_h(t)) \leq \|\mathbf{b}(t)\| \|\dot{\mathbf{u}}_h(t)\|. \quad (39)$$

We also have

$$\|\dot{\mathbf{u}}_h(t)\| \leq 2 \sqrt{\frac{1}{2} \|\dot{\mathbf{u}}_h\|^2 + PD^e(\mathbf{u}_h(t))} = 2 \sqrt{\mathcal{E}^e(\mathbf{u}_h)(t)},$$

where we use the fact that $PD^\epsilon(\mathbf{u})(t)$ is nonnegative. We substitute above inequality in Eq. 39 to get

$$\frac{d}{dt} \mathcal{E}^\epsilon(\mathbf{u}_h)(t) \leq 2\sqrt{\mathcal{E}^\epsilon(\mathbf{u}_h)(t)} \|\mathbf{b}(t)\|.$$

We fix $\delta > 0$ and define $A(t)$ as $A(t) = \mathcal{E}^\epsilon(\mathbf{u}_h)(t) + \delta$. Then, from the above equation, we easily have

$$\frac{d}{dt} A(t) \leq 2\sqrt{A(t)} \|\mathbf{b}(t)\| \Rightarrow \frac{1}{2} \frac{\frac{d}{dt} A(t)}{\sqrt{A(t)}} \leq \|\mathbf{b}(t)\|.$$

Noting that $\frac{1}{\sqrt{a(t)}} \frac{da(t)}{dt} = 2 \frac{d}{dt} \sqrt{a(t)}$, integrating from $t = 0$ to τ and relabeling τ as t , we get

$$\sqrt{A(t)} \leq \sqrt{A(0)} + \int_0^t \|\mathbf{b}(s)\| ds.$$

Proof is complete once we let $\delta \rightarrow 0$ and take the square of both sides.

4 Central Difference Time Discretization

In Sect. 4.2, we calculate the convergence rate for the central difference time discretization of the fully nonlinear problem. We then present a CFL-like condition on the time step Δt for the linearized peridynamic equation in Sect. 4.3.

At time step k , the exact solution is given by $(\mathbf{u}^k, \mathbf{v}^k)$, where $\mathbf{v}^k = \partial \mathbf{u}^k / \partial t$, and their projection onto V_h is given by $(\mathbf{r}_h(\mathbf{u}^k), \mathbf{r}_h(\mathbf{v}^k))$. The solution of fully discrete problem at time step k is given by $(\mathbf{u}_h^k, \mathbf{v}_h^k)$.

We approximate the initial data on displacement \mathbf{u}_0 and the velocity \mathbf{v}_0 by their projections $\mathbf{r}_h(\mathbf{u}_0)$ and $\mathbf{r}_h(\mathbf{v}_0)$. Let $\mathbf{u}_h^0 = \mathbf{r}_h(\mathbf{u}_0)$ and $\mathbf{v}_h^0 = \mathbf{r}_h(\mathbf{v}_0)$. For $k \geq 1$, $(\mathbf{u}_h^k, \mathbf{v}_h^k)$ satisfies, for all $\tilde{\mathbf{u}} \in V_h$,

$$\begin{cases} \left(\frac{\mathbf{u}_h^{k+1} - \mathbf{u}_h^k}{\Delta t}, \tilde{\mathbf{u}} \right) = (\mathbf{v}_h^{k+1}, \tilde{\mathbf{u}}), \\ \left(\frac{\mathbf{v}_h^{k+1} - \mathbf{v}_h^k}{\Delta t}, \tilde{\mathbf{u}} \right) = (\mathcal{L}^\epsilon(\mathbf{u}_h^k), \tilde{\mathbf{u}}) + (\mathbf{b}_h^k, \tilde{\mathbf{u}}), \end{cases} \quad (40)$$

where we have denoted the projection of $\mathbf{b}(t^k)$, i.e., $\mathbf{r}_h(\mathbf{b}(t^k))$, as \mathbf{b}_h^k . Combining the two equations delivers central difference equation for \mathbf{u}_h^k . We have

$$\left(\frac{\mathbf{u}_h^{k+1} - 2\mathbf{u}_h^k + \mathbf{u}_h^{k-1}}{\Delta t^2}, \tilde{\mathbf{u}} \right) = (\mathcal{L}^\epsilon(\mathbf{u}_h^k), \tilde{\mathbf{u}}) + (\mathbf{b}_h^k, \tilde{\mathbf{u}}), \quad \forall \tilde{\mathbf{u}} \in V_h. \quad (41)$$

For $k = 0$, we have $\forall \tilde{\mathbf{u}} \in V_h$,

$$\left(\frac{\mathbf{u}_h^1 - \mathbf{u}_h^0}{\Delta t^2}, \tilde{\mathbf{u}} \right) = \frac{1}{2}(\mathcal{L}^e(\mathbf{u}_h^0), \tilde{\mathbf{u}}) + \frac{1}{\Delta t}(\mathbf{v}_h^0, \tilde{\mathbf{u}}) + \frac{1}{2}(\mathbf{b}_h^0, \tilde{\mathbf{u}}). \quad (42)$$

4.1 Implementation Details

For completeness, we describe the implementation of the time stepping method using FEM interpolants. Let N be the shape tensor. Then, $\mathbf{u}_h^k, \tilde{\mathbf{u}} \in V_h$ are given by

$$\mathbf{u}_h^k = \mathbf{N}\mathbf{U}^k, \quad \tilde{\mathbf{u}} = \mathbf{N}\tilde{\mathbf{U}}, \quad (43)$$

where \mathbf{U}^k and $\tilde{\mathbf{U}}$ are Nd -dimensional vectors, where N is the number of nodal points in the mesh and d is the dimension.

From Eq. 41, for all $\tilde{\mathbf{U}} \in \mathbb{R}^{Nd}$ with elements of $\tilde{\mathbf{U}}$ zero on the boundary, then the following holds for $k \geq 1$:

$$\left(\mathbf{M} \frac{\mathbf{U}^{k+1} - 2\mathbf{U}^k + \mathbf{U}^{k-1}}{\Delta t^2} \right) \cdot \tilde{\mathbf{U}} = \mathbf{F}^k \cdot \tilde{\mathbf{U}}. \quad (44)$$

Here the mass matrix \mathbf{M} and the force vector \mathbf{F}^k are given by

$$\begin{cases} \mathbf{M} := \int_D \mathbf{N}^T \mathbf{N} d\mathbf{x}, \\ \mathbf{F}^k := \mathbf{F}_{pd}^k + \int_D \mathbf{N}^T \mathbf{b}(\mathbf{x}, t^k) d\mathbf{x}, \end{cases} \quad (45)$$

where \mathbf{F}_{pd}^k is defined by

$$\mathbf{F}_{pd}^k := \int_D \mathbf{N}^T (\mathcal{L}^e(\mathbf{u}_h^k)(\mathbf{x})) d\mathbf{x}. \quad (46)$$

We remark that a similar equation holds for $k = 0$.

At the time step k , we must invert \mathbf{M} to solve for \mathbf{U}^{k+1} using

$$\mathbf{U}^{k+1} = \Delta t^2 \mathbf{M}^{-1} \mathbf{F}^k + 2\mathbf{U}^k - \mathbf{U}^{k-1}. \quad (47)$$

As is well known, this inversion amounts to an increase of computational complexity associated with discrete approximation of the weak formulation of the evolution. Further, the matrix–vector multiplication $\mathbf{M}^{-1} \mathbf{F}^k$ needs to be carried out at each time step. On the other hand, the quadrature error in the computation of the force vector \mathbf{F}_{pd}^k is reduced when using the weak form.

We next show the convergence of approximation.

4.2 Convergence of Approximation

In this section, we prove the uniform bound on the error and show that the approximate solution converges to the exact solution with rate given by $C_t \Delta t + C_s h^2 / \epsilon^2$. Here the horizon $\epsilon > 0$ is assumed to be fixed. We first compare the exact solution with its projection in V_h and then compare the projection with the approximate solution. We further divide the calculation

of error between the projection and the approximate solution in two parts, namely the consistency analysis and error analysis.

The error E^k is given by

$$E^k := \|\mathbf{u}_h^k - \mathbf{u}(t^k)\| + \|\mathbf{v}_h^k - \mathbf{v}(t^k)\|.$$

The error is split into two parts as follows:

$$E^k \leq (\|\mathbf{u}^k - \mathbf{r}_h(\mathbf{u}^k)\| + \|\mathbf{v}^k - \mathbf{r}_h(\mathbf{v}^k)\|) + (\|\mathbf{r}_h(\mathbf{u}^k) - \mathbf{u}_h^k\| + \|\mathbf{r}_h(\mathbf{v}^k) - \mathbf{v}_h^k\|),$$

where the first term is the error between the exact solution and projection, and the second term is the error between the projection and approximate solution. Let

$$\mathbf{e}_h^k(\mathbf{u}) := \mathbf{r}_h(\mathbf{u}^k) - \mathbf{u}_h^k, \quad \mathbf{e}_h^k(\mathbf{v}) := \mathbf{r}_h(\mathbf{v}^k) - \mathbf{v}_h^k, \quad (48)$$

and

$$e^k := \|\mathbf{e}_h^k(\mathbf{u})\| + \|\mathbf{e}_h^k(\mathbf{v})\|. \quad (49)$$

Using Eq. 37, we have

$$E^k \leq C_p h^2 + e^k, \quad (50)$$

where

$$C_p := c \left(\sup_t \|\mathbf{u}(t)\|_2 + \sup_t \left\| \frac{\partial \mathbf{u}(t)}{\partial t} \right\|_2 \right). \quad (51)$$

We have the following a-priori convergence rate given by

Theorem 5 (Convergence of central difference approximation) *Let (\mathbf{u}, \mathbf{v}) be the exact solution of the peridynamic Eq. 11 and $(\mathbf{u}_h^k, \mathbf{v}_h^k)$ be the FE solution of Eq. 40. If $\mathbf{u}, \mathbf{v} \in C^2([0, T]; W)$, then the scheme is consistent and the error E^k satisfies the following bound:*

$$\begin{aligned} & \sup_{k \leq T/\Delta t} E^k \\ &= C_p h^2 + \exp \left[T \left(1 + \frac{L^2}{\epsilon} \right) \left(\frac{1}{1 - \Delta t} \right) \right] \left[e^0 + \left(\frac{T}{1 - \Delta t} \right) \left(C_t \Delta t + C_s \frac{h^2}{\epsilon^2} \right) \right], \end{aligned} \quad (52)$$

where the constants C_p , C_t , and C_s are given by Eqs. 51 and 58. The constant L/ϵ^2 is the Lipschitz constant of the peridynamic force $\mathcal{L}^\epsilon(\mathbf{u})$ in L^2 ; see Eq. 23. If the error in initial data is zero, then E^k is of the order of $C_t \Delta t + C_s h^2/\epsilon^2$.

In Theorem 3, we have shown that $\mathbf{u}, \mathbf{v} \in C^2([0, T]; W)$ for righthand side $\mathbf{b} \in C^1([0, T]; W)$. In Sect. 7, we discuss the behavior of the exponential constant appearing in Theorem 5 for evolution times seen in fracture experiments. Since we are approximating the solution of an ODE on a Banach space, the proof of Theorem 5 will follow from the Lipschitz continuity of the force $\mathcal{L}^\epsilon(\mathbf{u})$ with respect to the L^2 norm. The proof is given in the following two sections.

4.2.1 Truncation Error Analysis and Consistency

The results in this section follow the same steps as in [20] and, therefore, we will just highlight the major steps. We can write the discrete evolution equation for ($e_h^k(\mathbf{u}) = \mathbf{r}_h(\mathbf{u}^k) - \mathbf{u}_h^k$, $e_h^k(\mathbf{v}) = \mathbf{r}_h(\mathbf{v}^k) - \mathbf{v}_h^k$) as follows:

$$\begin{cases} (e_h^{k+1}(\mathbf{u}), \tilde{\mathbf{u}}) = (e_h^k(\mathbf{u}), \tilde{\mathbf{u}}) + \Delta t(e_h^{k+1}(\mathbf{v}), \tilde{\mathbf{u}}) + \Delta t(\tau_h^k(\mathbf{u}), \tilde{\mathbf{u}}), \\ (e_h^{k+1}(\mathbf{v}), \tilde{\mathbf{u}}) = (e_h^k(\mathbf{v}), \tilde{\mathbf{u}}) + \Delta t(\mathcal{L}^\epsilon(\mathbf{u}_h^k) - \mathcal{L}^\epsilon(\mathbf{r}_h(\mathbf{u}^k)), \tilde{\mathbf{u}}) \\ \quad + \Delta t(\tau_h^k(\mathbf{v}), \tilde{\mathbf{u}}) + \Delta t(\sigma_h^k(\mathbf{u}), \tilde{\mathbf{u}}), \end{cases} \quad (53)$$

where consistency error terms $\tau_h^k(\mathbf{u})$, $\tau_h^k(\mathbf{v})$, $\sigma_h^k(\mathbf{u})$ are given by

$$\begin{cases} \tau_h^k(\mathbf{u}) := \frac{\partial \mathbf{u}^{k+1}}{\partial t} - \frac{\mathbf{u}^{k+1} - \mathbf{u}^k}{\Delta t}, \\ \tau_h^k(\mathbf{v}) := \frac{\partial \mathbf{v}^k}{\partial t} - \frac{\mathbf{v}^{k+1} - \mathbf{v}^k}{\Delta t}, \\ \sigma_h^k(\mathbf{u}) := \mathcal{L}^\epsilon(\mathbf{r}_h(\mathbf{u}^k)) - \mathcal{L}^\epsilon(\mathbf{u}^k). \end{cases} \quad (54)$$

When \mathbf{u} , \mathbf{v} are C^2 in time, we easily see that

$$\|\tau_h^k(\mathbf{u})\| \leq \Delta t \sup_t \left\| \frac{\partial^2 \mathbf{u}}{\partial t^2} \right\| \quad \text{and} \quad \|\tau_h^k(\mathbf{v})\| \leq \Delta t \sup_t \left\| \frac{\partial^2 \mathbf{v}}{\partial t^2} \right\|.$$

To estimate $\sigma_h^k(\mathbf{u})$, we recall the Lipschitz continuity property of the peridynamic force in the L^2 norm; see Eq. 23. This leads us to

$$\|\sigma_h^k(\mathbf{u})\| \leq \frac{L}{\epsilon^2} \|\mathbf{u}^k - \mathbf{r}_h(\mathbf{u}^k)\| \leq \frac{Lc}{\epsilon^2} h^2 \sup_t \|\mathbf{u}(t)\|_2, \quad (55)$$

where the constant L is defined in Eq. 24.

We now state the consistency of this approach.

Lemma 2 (Consistency) *Let τ be given by*

$$\tau := \sup_k (\|\tau_h^k(\mathbf{u})\| + \|\tau_h^k(\mathbf{v})\| + \|\sigma_h^k(\mathbf{u})\|). \quad (56)$$

Then, the approach is consistent in that

$$\tau \leq C_i \Delta t + C_s \frac{h^2}{\epsilon^2}, \quad (57)$$

where

$$C_i := \left\| \frac{\partial^2 \mathbf{u}}{\partial t^2} \right\| + \left\| \frac{\partial^2 \mathbf{v}}{\partial t^2} \right\| \quad \text{and} \quad C_s := Lc \sup_t \|\mathbf{u}(t)\|_2. \quad (58)$$

4.2.2 Stability Analysis

In equation for $\mathbf{e}_h^k(\mathbf{u})$, we take $\tilde{\mathbf{u}} = \mathbf{e}_h^{k+1}(\mathbf{u})$. We have

$$||\mathbf{e}_h^{k+1}(\mathbf{u})||^2 = (\mathbf{e}_h^k(\mathbf{u}), \mathbf{e}_h^{k+1}(\mathbf{u})) + \Delta t(\mathbf{e}_h^{k+1}(\mathbf{v}), \mathbf{e}_h^{k+1}(\mathbf{u})) + \Delta t(\boldsymbol{\tau}_h^k(\mathbf{u}), \mathbf{e}_h^{k+1}(\mathbf{u})),$$

which implies

$$||\mathbf{e}_h^{k+1}(\mathbf{u})|| \leq ||\mathbf{e}_h^k(\mathbf{u})|| + \Delta t||\mathbf{e}_h^{k+1}(\mathbf{v})|| + \Delta t||\boldsymbol{\tau}_h^k(\mathbf{u})||. \quad (59)$$

Similarly, we can show

$$\begin{aligned} ||\mathbf{e}_h^{k+1}(\mathbf{v})|| &\leq ||\mathbf{e}_h^k(\mathbf{v})|| + \Delta t||\mathcal{L}^e(\mathbf{u}_h^k) - \mathcal{L}^e(\mathbf{r}_h(\mathbf{u}^k))|| \\ &\quad + \Delta t \left(||\boldsymbol{\tau}_h^k(\mathbf{v})|| + ||\boldsymbol{\sigma}_{per,h}^k(\mathbf{u})|| \right). \end{aligned} \quad (60)$$

We have from Eq. 23

$$||\mathcal{L}^e(\mathbf{u}_h^k) - \mathcal{L}^e(\mathbf{r}_h(\mathbf{u}^k))|| \leq \frac{L}{\epsilon^2} ||\mathbf{u}_h^k - \mathbf{r}_h(\mathbf{u}^k)|| = \frac{L}{\epsilon^2} ||\mathbf{e}_h^k(\mathbf{u})||. \quad (61)$$

After adding Eqs. 59 and 60, and substituting Eq. 61, we get

$$||\mathbf{e}_h^{k+1}(\mathbf{u})|| + ||\mathbf{e}_h^{k+1}(\mathbf{v})|| \leq ||\mathbf{e}_h^k(\mathbf{u})|| + ||\mathbf{e}_h^k(\mathbf{v})|| + \Delta t||\mathbf{e}_h^{k+1}(\mathbf{v})|| + \frac{L}{\epsilon^2} \Delta t ||\mathbf{e}_h^k(\mathbf{u})|| + \Delta t \tau,$$

where τ is defined in Eq. 56. Since $e^k = ||\mathbf{e}_h^k(\mathbf{u})|| + ||\mathbf{e}_h^k(\mathbf{v})||$, we can show, assuming $L/\epsilon^2 \geq 1$,

$$\begin{aligned} e^{k+1} &\leq e^k + \Delta t e^{k+1} + \Delta t \frac{L}{\epsilon^2} e^k + \Delta t \tau \\ \Rightarrow e^{k+1} &\leq \frac{1 + \frac{\Delta t L}{\epsilon^2}}{1 - \Delta t} e^k + \frac{\Delta t}{1 - \Delta t} \tau. \end{aligned}$$

Substituting for e^k recursively in the equation above, we get

$$e^{k+1} \leq \left(\frac{1 + \frac{\Delta t L}{\epsilon^2}}{1 - \Delta t} \right)^{k+1} e^0 + \frac{\Delta t}{1 - \Delta t} \tau \sum_{j=0}^k \left(\frac{1 + \frac{\Delta t L}{\epsilon^2}}{1 - \Delta t} \right)^{k-j}.$$

Noting that

$$\frac{1 + \frac{\Delta t L}{\epsilon^2}}{1 - \Delta t} = 1 + \frac{1 + \frac{L}{\epsilon^2}}{1 - \Delta t} \Delta t$$

and $(1 + a\Delta t)^k \leq \exp(ka\Delta t) \leq \exp(Ta)$ for $a > 0$, we have

$$\left(\frac{1 + \frac{\Delta t L_1}{\epsilon^2}}{1 - \Delta t} \right)^k \leq \exp \left[\frac{T \left(1 + \frac{L_1}{\epsilon^2} \right)}{1 - \Delta t} \right]. \quad (62)$$

This implies

$$\begin{aligned}
e^{k+1} &\leq \exp \left[\frac{T \left(1 + \frac{L}{\epsilon^2} \right)}{1 - \Delta t} \right] \left(e^0 + \frac{\Delta t}{1 - \Delta t} \tau \sum_{j=0}^k 1 \right) \\
&\leq \exp \left[\frac{T \left(1 + \frac{L}{\epsilon^2} \right)}{1 - \Delta t} \right] \left(e^0 + \frac{k \Delta t}{1 - \Delta t} \tau \right).
\end{aligned}$$

By substituting above equation in Eq. 50, we get the stability of the scheme.

Lemma 3 (Stability)

$$E^k \leq C_p h^2 + \exp \left[\frac{T \left(1 + \frac{L}{\epsilon^2} \right)}{1 - \Delta t} \right] \left(e^0 + \frac{k \Delta t}{1 - \Delta t} \tau \right). \quad (63)$$

After taking sup over $k \leq T/\Delta t$ and substituting the bound on τ from Lemma 2, we get the desired result and proof of Theorem 5 is complete.

We now consider a stronger notion of stability for the linearized peridynamics model.

4.3 Linearized Peridynamics and Energy Stability

In this section, we linearize the peridynamics model and obtain a CFL-like stability condition. For problems, where strains are small, the stability condition for the linearized model is expected to apply to the nonlinear model. The slope of peridynamics potential f and g are constant for sufficiently small strain and, therefore, for small strain, the nonlinear model behaves like a linear model.

In Eq. 13, the linearization gives

$$\mathcal{L}_{T,l}^\epsilon(\mathbf{u})(\mathbf{x}) = \frac{2}{\epsilon^{d+1} \omega_d} \int_{H_\epsilon(\mathbf{x})} \omega(\mathbf{x}) \omega(\mathbf{y}) J^\epsilon(|\mathbf{y} - \mathbf{x}|) f''(0) S(\mathbf{y}, \mathbf{x}; \mathbf{u}) \mathbf{e}_{y-x} d\mathbf{y}. \quad (64)$$

The corresponding bilinear form is denoted as $a_{T,l}^\epsilon$ and is given by

$$a_{T,l}^\epsilon(\mathbf{u}, \mathbf{v}) = \frac{f''(0)}{\epsilon^{d+1} \omega_d} \int_D \int_D \omega(\mathbf{x}) \omega(\mathbf{y}) J^\epsilon(|\mathbf{y} - \mathbf{x}|) |\mathbf{y} - \mathbf{x}| S(\mathbf{y}, \mathbf{x}; \mathbf{u}) S(\mathbf{y}, \mathbf{x}; \mathbf{v}) d\mathbf{y} d\mathbf{x}. \quad (65)$$

Similarly, the linearization of \mathcal{L}_D^ϵ in Eq. 14 gives

$$\mathcal{L}_{D,l}^\epsilon(\mathbf{u})(\mathbf{x}) = \frac{g''(0)}{\epsilon^{d+2} \omega_d} \int_{H_\epsilon(\mathbf{x})} \omega(\mathbf{x}) \omega(\mathbf{y}) J^\epsilon(|\mathbf{y} - \mathbf{x}|) [\theta(\mathbf{y}, t; \mathbf{u}) + \theta(\mathbf{x}, t; \mathbf{u})] \mathbf{e}_{y-x} d\mathbf{y}. \quad (66)$$

The associated bilinear form is given by

$$a_{D,l}^\epsilon(\mathbf{u}, \mathbf{v}) = \frac{g''(0)}{\epsilon^2} \int_D \omega(\mathbf{x}) \theta(\mathbf{x}; \mathbf{u}) \theta(\mathbf{y}; \mathbf{v}) d\mathbf{x}. \quad (67)$$

The total force after linearization is

$$\mathcal{L}_l^\epsilon(\mathbf{u})(\mathbf{x}) = \mathcal{L}_{T,l}^\epsilon(\mathbf{u})(\mathbf{x}) + \mathcal{L}_{D,l}^\epsilon(\mathbf{u})(\mathbf{x}) \quad (68)$$

and the bilinear operator associated with \mathcal{L}_l^ϵ is given by

$$a_l^\epsilon(\mathbf{u}, \mathbf{v}) = a_{T,l}^\epsilon(\mathbf{u}, \mathbf{v}) + a_{D,l}^\epsilon(\mathbf{u}, \mathbf{v}). \quad (69)$$

We have

$$(\mathcal{L}_l^\epsilon(\mathbf{u}), \mathbf{v}) = -a_l^\epsilon(\mathbf{u}, \mathbf{v}).$$

We now discuss the stability of the FEM approximation to the linearized problem. Let $\mathbf{u}_{l,h}^k$ denote the approximate solution satisfying, for $k \geq 1$,

$$\left(\frac{\mathbf{u}_{l,h}^{k+1} - 2\mathbf{u}_{l,h}^k + \mathbf{u}_{l,h}^{k-1}}{\Delta t^2}, \tilde{\mathbf{u}} \right) = (\mathcal{L}_l^\epsilon(\mathbf{u}_{l,h}^k), \tilde{\mathbf{u}}) + (\mathbf{b}_h^k, \tilde{\mathbf{u}}), \quad \forall \tilde{\mathbf{u}} \in V_h \quad (70)$$

and, for $k = 0$,

$$\left(\frac{\mathbf{u}_{l,h}^1 - \mathbf{u}_{l,h}^0}{\Delta t^2}, \tilde{\mathbf{u}} \right) = \frac{1}{2}(\mathcal{L}_l^\epsilon(\mathbf{u}_{l,h}^0), \tilde{\mathbf{u}}) + \frac{1}{\Delta t}(\mathbf{v}_{l,h}^0, \tilde{\mathbf{u}}) + \frac{1}{2}(\mathbf{b}_h^0, \tilde{\mathbf{u}}), \quad \forall \tilde{\mathbf{u}} \in V_h. \quad (71)$$

The following notation will be used to define the discrete energy at each time step k :

$$\begin{cases} \bar{\mathbf{u}}_h^{k+1} := \frac{\mathbf{u}_h^{k+1} + \mathbf{u}_h^k}{2}, \bar{\mathbf{u}}_h^k := \frac{\mathbf{u}_h^k + \mathbf{u}_h^{k-1}}{2}, \\ \bar{\partial}_t \mathbf{u}_h^k := \frac{\mathbf{u}_h^{k+1} - \mathbf{u}_h^{k-1}}{2\Delta t}, \bar{\partial}_t^+ \mathbf{u}_h^k := \frac{\mathbf{u}_h^{k+1} - \mathbf{u}_h^k}{\Delta t}, \bar{\partial}_t^- \mathbf{u}_h^k := \frac{\mathbf{u}_h^k - \mathbf{u}_h^{k-1}}{\Delta t}. \end{cases} \quad (72)$$

We also define

$$\bar{\partial}_t \mathbf{u}_h^k := \frac{\mathbf{u}_h^{k+1} - 2\mathbf{u}_h^k + \mathbf{u}_h^{k-1}}{\Delta t^2} = \frac{\bar{\partial}_t^+ \mathbf{u}_h^k - \bar{\partial}_t^- \mathbf{u}_h^k}{\Delta t}.$$

We introduce the discrete energy associated with $\mathbf{u}_{l,h}^k$ at time step k as follows:

$$\mathcal{E}(\mathbf{u}_{l,h}^k) := \frac{1}{2} \left[|\bar{\partial}_t^+ \mathbf{u}_{l,h}^k|^2 - \frac{\Delta t^2}{4} a_l^\epsilon(\bar{\partial}_t^+ \mathbf{u}_{l,h}^k, \bar{\partial}_t^+ \mathbf{u}_{l,h}^k) + a_l^\epsilon(\bar{\mathbf{u}}_{l,h}^{k+1}, \bar{\mathbf{u}}_{l,h}^{k+1}) \right].$$

Following [Theorem 4.1, [24]], the stability of central difference scheme is given by

Theorem 6 (Energy stability of the central difference approximation of linearized peridynamics) *Let $\mathbf{u}_{l,h}^k$ be the approximate solution of Eqs. 70 and 71. In the absence of body force $\mathbf{b}(t) = 0$ for all t , if Δt satisfies the CFL-like condition*

$$\frac{\Delta t^2}{4} \sup_{\mathbf{u} \in V_h \setminus \{0\}} \frac{a_l^\epsilon(\mathbf{u}, \mathbf{u})}{(\mathbf{u}, \mathbf{u})} \leq 1, \quad (73)$$

then the discrete energy is positive and we have the stability

$$\mathcal{E}(\mathbf{u}_{l,h}^k) = \mathcal{E}(\mathbf{u}_{l,h}^0). \quad (74)$$

We skip the proof of above theorem as it is straightforward extension of Theorem 5.2 in [20].

5 Numerical Experiments

In this section, we present numerical simulations that are consistent with the theoretical a-priori bound on the convergence rate. We also compare the peridynamic energy of the material softening zone and the classic Griffith's fracture energy of linear elastic fracture mechanics.

We consider Plexiglass at room temperature and specify the density $\rho = 1\,200 \text{ kg/m}^3$, the bulk modulus $K = 25 \text{ GPa}$, the Poisson's ratio $\nu = 0.245$, and the critical energy release rate $G_c = 500 \text{ Jm}^{-2}$. The pairwise interaction and the hydrostatic interaction are characterized by potentials $f(r) = c(1 - \exp(-\beta r^2))$ and $g(r) = \bar{C}r^2/2$, respectively. Here we have used a quadratic hydrostatic interaction potential. The influence function is $J(r) = 1 - r$. Since the pairwise potential f is symmetric for positive and negative strains, the critical strain is given by $S_c(\mathbf{y}, bx) = \frac{\pm\bar{r}}{\sqrt{y-x}}$, where $\pm\bar{r}$ is the inflection point of $f(r)$ given by $\bar{r} = \frac{1}{\sqrt{\beta}}$. Following Eqs. 94, 95, and 97 of [29], the relation between peridynamic material parameters and Lamé constants (λ, μ) and the critical energy release rate G_c can be written as (for 2-d)

$$c = \frac{\pi G_c}{4M_J}, \quad \beta = \frac{4\mu}{CM_J}, \quad \bar{C} = \frac{2(\lambda - \mu)}{M_J^2}, \quad (75)$$

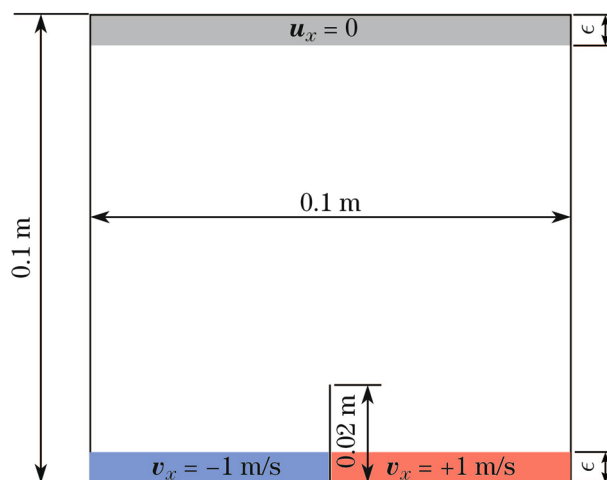
where M_J is given by

$$M_J = \int_0^1 J(r)r^2 dr = \frac{1}{12}.$$

By solving Eq. 75, we get $c = 4\,712.4$, $\bar{C} = -1.734\,9 \times 10^{11}$, $\beta = 1.564\,7 \times 10^8$.

We consider a 2-d domain $D = [0, 0.1 \text{ m}]^2$ (with unit thickness in third direction) with the vertical crack of length 0.02 m. The boundary conditions are described in Fig. 3. The

Fig. 3 Material domain $D = [0, 0.1 \text{ m}]^2$ with crack of length 0.02 m. The x -component and y -component of displacement are fixed along a collar of thickness equal to the horizon on top. On the bottom the velocity $v_x = \pm 1 \text{ m/s}$ along x -direction is specified on either side of the crack to make the crack propagate upwards



simulation time is $T = 40 \mu\text{s}$ and the time step is $\Delta t = 0.004 \mu\text{s}$. We consider two horizons 8 mm and 4 mm. We run simulations for mesh sizes $h = 2, 1, 0.5 \text{ mm}$. We consider the central difference time discretization described by Eq. 41 on a uniform mesh consisting of linear triangle elements. The second-order quadrature approximation is used in the simulation for each triangle element. To reduce the load on memory and to avoid the matrix–vector multiplication at each time step, we approximate the mass matrix by the diagonal mass matrix using the lumping (row-sum) technique. Suppose the exact mass matrix is $\mathbf{M} = [m_{ij}]$ where m_{ij} is the element of \mathbf{M} corresponding to i th row and j th column, then we approximate \mathbf{M} by the diagonal matrix $\hat{\mathbf{M}} = [\hat{m}_{ij}]$ where $\hat{m}_{ii} = \sum_j m_{ij}$ and $\hat{m}_{ij} = 0$ if $j \neq i$.

5.1 Convergence Rate

To compute the convergence rate numerically we proceed as follows: consider a fixed horizon ϵ and three different mesh sizes h_1, h_2, h_3 such that $r = h_1/h_2 = h_2/h_3$. Let $\mathbf{u}_1, \mathbf{u}_2, \mathbf{u}_3$ be approximate solutions corresponding to meshes of size h_1, h_2, h_3 , and let \mathbf{u} be the exact solution. We write the error as $\|\mathbf{u}_h - \mathbf{u}\| = Ch^\alpha$ for some constant C and $\alpha > 0$, to get

$$\log(\|\mathbf{u}_1 - \mathbf{u}_2\|) = C + \alpha \log h_2,$$

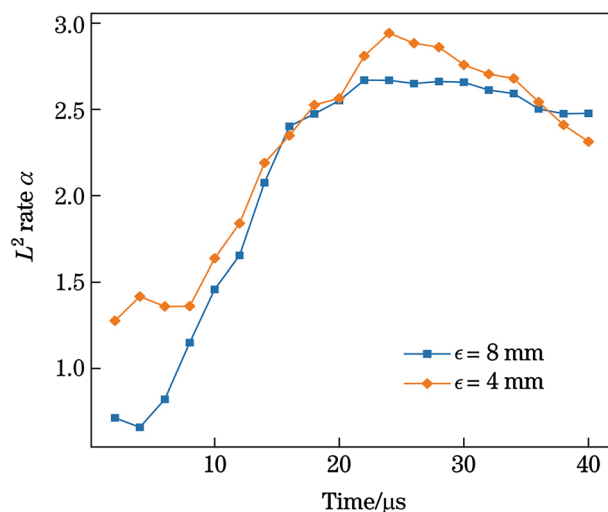
$$\log(\|\mathbf{u}_2 - \mathbf{u}_3\|) = C + \alpha \log h_3.$$

From the above two equations, it is easy to see that the rate of convergence α is

$$\frac{\log(\|\mathbf{u}_1 - \mathbf{u}_2\|) - \log(\|\mathbf{u}_2 - \mathbf{u}_3\|)}{\log(r)}. \quad (76)$$

The convergence result for horizons $\epsilon = 8 \text{ mm}$ and $\epsilon = 4 \text{ mm}$ is shown in Fig. 4. In the simulation, we have considered the second-order approximation of integration using quadrature points. The simulations show a rate of convergence that agrees with the a priori estimates given in Theorem 6.

Fig. 4 Convergence rate at different times for two horizons. For both horizons $\epsilon = 4, 8 \text{ mm}$, the three meshes of size $h = 2, 1, 0.5 \text{ mm}$ were considered to compute the convergence rate



5.2 Fracture Energy of Crack Zone

The extent of damage at material point x is given by the function $Z(x)$

$$Z(x) = \max_{y \in H_\epsilon(x) \cap D} \frac{S(y, x; \mathbf{u})}{S_c^+}. \quad (77)$$

The crack zone is defined as set of material points which have $Z > 1$. We compute the peridynamic energy of crack zone and compare it with the Griffith's fracture energy. For a crack of length l , the Griffith's fracture energy (G.E.) will be $G.E. = G_c \times l$. The peridynamic fracture energy (P.E.) associated with the material softening zone is given by

$$\begin{aligned} P.E. = & \int_{\substack{x \in D, \\ Z(x) \geq 1}} \left[\frac{1}{\epsilon^d \omega_d} \int_{H_\epsilon(x)} |y - x| \mathcal{W}^\epsilon(S(y, x; \mathbf{u})) dy \right] dx \\ & + \int_{\substack{x \in D, \\ Z(x) \geq 1}} \mathcal{V}^\epsilon(\theta(x, t; \mathbf{u})) dx, \end{aligned}$$

where $\mathcal{W}^\epsilon(S(y, x; \mathbf{u}))$ is the bond-based potential; see Eq. 2 and $\mathcal{V}^\epsilon(\theta(x, t; \mathbf{u}))$ is the hydrostatic interaction potential; see Eq. 4.

In Fig. 5, the classical fracture energy and the peridynamic fracture energy are shown at different crack lengths. The error in both energies at different times is shown in Fig. 6. The agreement between two energies is good. The damage profile at time 30 μ s and 40 μ s is shown in Fig. 7. At each node, the damage function Z is computed by treating edges between mesh nodes as bonds. In addition to the damage plots, we show the velocity profile at 30 μ s and 40 μ s in Fig. 8. In Fig. 9, we show the plot of the xx component of symmetric gradient of the displacement. Here the region for which the magnitude of the strain is greater than a multiple of the critical strain is the yellow region. It is seen that the high-strain region surrounds the crack.

As the crack is propagating vertically it is seen that the high-strain region is next to the crack.

6 Lipschitz Continuity of Peridynamic Force and Higher Temporal Regularity of Solutions

In this section, we prove Theorems 1 and 3. Here $\mathbf{u} \in W \subset H^2(D; \mathbb{R}^d)$ and the $\|\mathbf{u}\|_2$ norm is given by

$$\|\mathbf{u}\|_2 = \|\mathbf{u}\| + \|\nabla \mathbf{u}\| + \|\nabla^2 \mathbf{u}\|. \quad (78)$$

6.1 Proof of Lipschitz Continuity with Respect to the $\|\cdot\|_2$ Norm

We assume that the potential function f satisfies $C_i^f < \infty$ for $i = 0, 1, 2, 3, 4$. Recall that $C_0^f = \sup_r |f(r)|$ and $C_i^f = \sup_r |f^{(r)}(r)|$ for $i = 1, \dots, 4$. C_i^g is defined similarly for $i = 0, 1, \dots, 4$. If the potential function g is a convex-concave function, then we can

Fig. 5 Peridynamic energy and Griffith's energy as a function of crack length

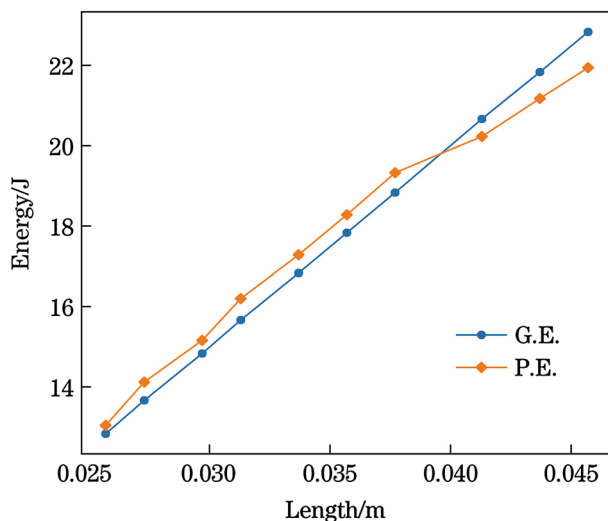
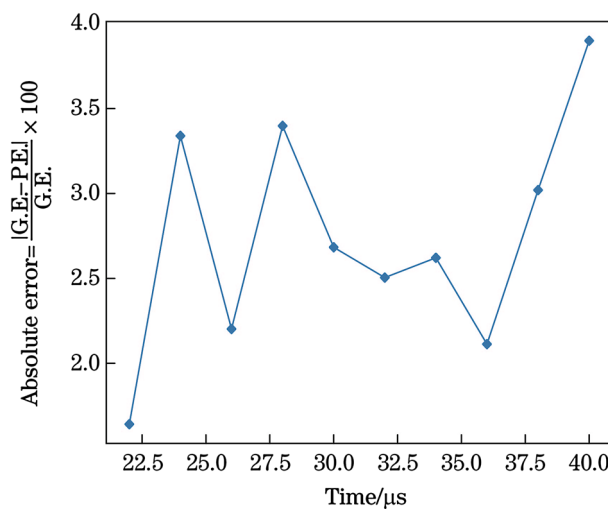


Fig. 6 Error between Peridynamic energy and Griffith's energy at different times



assume $C_i^g < \infty$ for $i = 0, 1, 2, 3, 4$. In what follows, we will prove Theorem 1 for convex–concave type g . If g is a purely a quadratic function, the proof follows easily using only a subset of the estimates proved in this section.

Let $\mathbf{u}, \mathbf{v} \in W$. Using the triangle inequality, we get

$$\|\mathcal{L}^\epsilon(\mathbf{u}) - \mathcal{L}^\epsilon(\mathbf{v})\|_2 \leq \|\mathcal{L}_T^\epsilon(\mathbf{u}) - \mathcal{L}_T^\epsilon(\mathbf{v})\|_2 + \|\mathcal{L}_D^\epsilon(\mathbf{u}) - \mathcal{L}_D^\epsilon(\mathbf{v})\|_2, \quad (79)$$

where \mathcal{L}_T^ϵ and \mathcal{L}_D^ϵ is given by Eqs. 13 and 14.

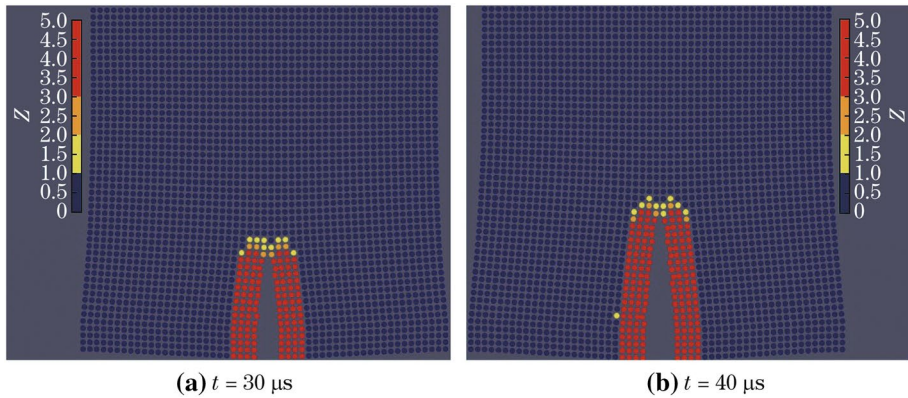


Fig. 7 Color plot of damage function Z on deformed material domain at time $t = 30 \mu\text{s}$ and $40 \mu\text{s}$. Dark blue represents undamaged material $Z < 1$, $Z \approx 1$ is yellow at crack tip, red is softening material. Here, the displacements are scaled by 100 and damage function is cut off at 5 to highlight the crack zone

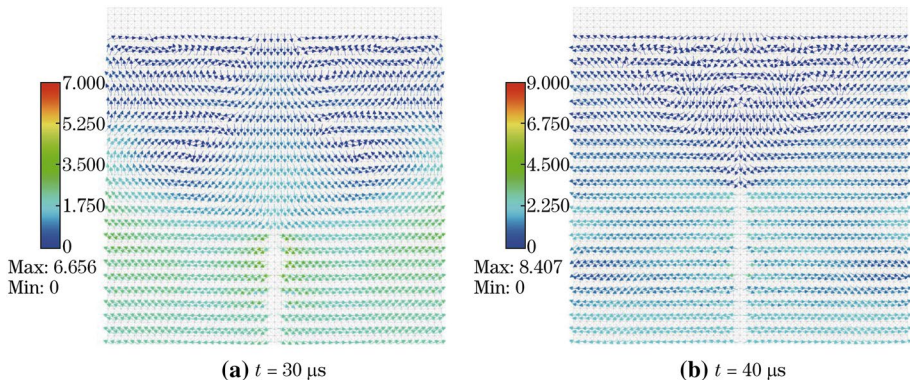


Fig. 8 Velocity profile

We first write the peridynamic force $\mathcal{L}_T^\epsilon(\mathbf{u})(\mathbf{x})$ as follows:

$$\begin{aligned} \mathcal{L}_T^\epsilon(\mathbf{u})(\mathbf{x}) &= \frac{2}{\epsilon^{d+1} \omega_d} \int_{H_\epsilon(\mathbf{x})} \omega(\mathbf{x}) \omega(\mathbf{y}) \frac{J^\epsilon(|\mathbf{y} - \mathbf{x}|)}{\sqrt{|\mathbf{y} - \mathbf{x}|}} f'(\sqrt{|\mathbf{y} - \mathbf{x}|} S(\mathbf{y}, \mathbf{x}; \mathbf{u})) \mathbf{e}_{\mathbf{y}-\mathbf{x}} \, d\mathbf{y}, \end{aligned} \quad (80)$$

where we substitute $\partial_S f(\sqrt{|\mathbf{y} - \mathbf{x}|} S(\mathbf{y}, \mathbf{x}; \mathbf{u})) = \sqrt{|\mathbf{y} - \mathbf{x}|} f'(\sqrt{|\mathbf{y} - \mathbf{x}|} S(\mathbf{y}, \mathbf{x}; \mathbf{u}))$. The form of the peridynamic force described above is the same as the one given in [Section 6, [20]]. We apply Theorem 3.1 in [20] to show

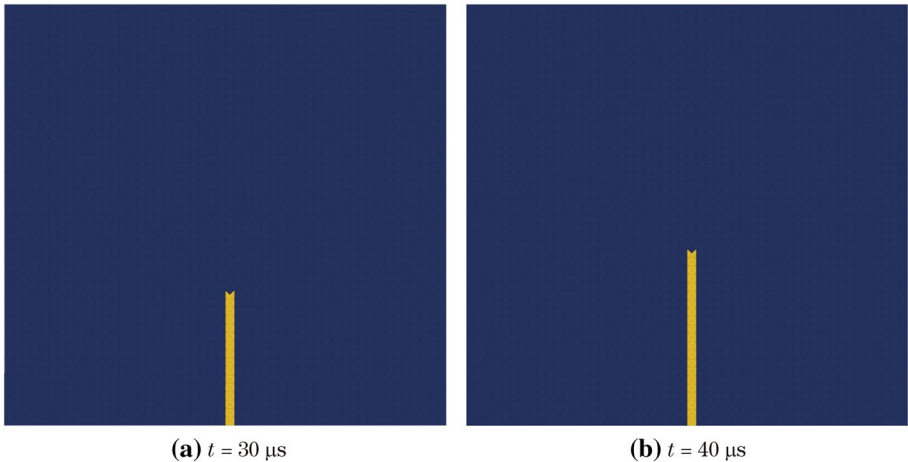


Fig. 9 Magnitude of the xx component of strain $\nabla\mathbf{u} + \nabla\mathbf{u}^T$. The region for which the magnitude of the strain is greater than a multiple of the critical strain is the yellow region

$$\begin{aligned} \|\mathcal{L}_T^\epsilon(\mathbf{u}) - \mathcal{L}_T^\epsilon(\mathbf{v})\|_2 &\leq \frac{L_1(1 + (\|\mathbf{u}\|_2 + \|\mathbf{v}\|_2) + (\|\mathbf{u}\|_2 + \|\mathbf{v}\|_2)^2)}{\epsilon^3} \|\mathbf{u} - \mathbf{v}\|_2 \\ &\leq \frac{L_1(1 + \|\mathbf{u}\|_2 + \|\mathbf{v}\|_2)^2}{\epsilon^3} \|\mathbf{u} - \mathbf{v}\|_2 \end{aligned} \quad (81)$$

and

$$\|\mathcal{L}_T^\epsilon(\mathbf{u})\|_2 \leq \frac{L_2(\|\mathbf{u}\|_2 + \|\mathbf{u}\|_2^2)}{\epsilon^{5/2}}. \quad (82)$$

Next we analyze $\|\mathcal{L}_D^\epsilon(\mathbf{u}) - \mathcal{L}_D^\epsilon(\mathbf{v})\|_2$. We define new terms to simplify the calculations. For $\xi \in H_1(\mathbf{0})$, we set

$$\begin{cases} s_\xi = \epsilon|\xi|, e_\xi = \frac{\xi}{|\xi|}, \\ \omega_\xi(x) = \omega(x + \epsilon\xi)\omega(x), \\ \bar{u}_\xi(x) = u(x + \epsilon\xi) - u(x), \\ (u - v)(x) = u(x) - v(x). \end{cases} \quad (83)$$

Similar notations hold if we exchange $x, \xi \in H_1(\mathbf{0})$, and $\mathbf{u} \in W$ by $y, \eta \in H_1(\mathbf{0})$, and $\mathbf{v} \in W$, respectively. We will also encounter various moments of the influence function J ; therefore, we define the following moments:

$$\bar{J}_\alpha = \frac{1}{\omega_d} \int_{H_1(\mathbf{0})} J(|\xi|)|\xi|^{-\alpha} d\xi \quad \text{for } \alpha \in \mathbb{R}. \quad (84)$$

Recall that $J(|\xi|) = 0$ for $\xi \notin H_1(\mathbf{0})$ and $0 \leq J(|\xi|) \leq M$ for $\xi \in H_1(\mathbf{0})$. The boundary function ω is assumed to satisfy

$$\sup_x |\nabla \omega(\mathbf{x})| < \infty, \quad \sup_x |\nabla^2 \omega(\mathbf{x})| < \infty. \quad (85)$$

We choose finite constants C_{ω_1} and C_{ω_2} such that

$$\begin{cases} |\nabla \omega_\xi(\mathbf{x})| \leq C_{\omega_1}, & |\nabla \omega(\mathbf{x})| \leq C_{\omega_1}, \\ |\nabla^2 \omega_\xi(\mathbf{x})| \leq C_{\omega_2}, & |\nabla^2 \omega(\mathbf{x})| \leq C_{\omega_2}. \end{cases} \quad (86)$$

We now collect the following estimates which will be used to estimate $\|\mathcal{L}_D^c(\mathbf{u}) - \mathcal{L}_D^c(\mathbf{v})\|_2$.

Lemma 4 *Let $\mathbf{u}, \mathbf{v} \in W$, for any $\boldsymbol{\eta} \in H_1(\mathbf{0})$ and $\delta \leq 2\epsilon$, we have*

$$\sup_{x \in D} |\theta(\mathbf{x}; \mathbf{u})| \leq 2C_{e_1} \bar{J}_0 \|\mathbf{u}\|_2, \quad (87)$$

$$\int_D |\theta(\mathbf{x} + \delta \boldsymbol{\eta}; \mathbf{u})|^2 d\mathbf{x} \leq 4\bar{J}_0^2 \|\mathbf{u}\|_2^2, \quad (88)$$

$$\int_D |\nabla \theta(\mathbf{x} + \delta \boldsymbol{\eta}; \mathbf{u})|^2 d\mathbf{x} \leq 8\bar{J}_0^2 (1 + C_{\omega_1})^2 \|\mathbf{u}\|_2^2, \quad (89)$$

$$\int_D |\theta(\mathbf{x} + \delta \boldsymbol{\eta}; \mathbf{u} - \mathbf{v})|^2 |\nabla \theta(\mathbf{x} + \delta \boldsymbol{\eta}; \mathbf{v})|^2 d\mathbf{x} \leq 32\bar{J}_0^4 (1 + C_{\omega_1})^2 \|\mathbf{v}\|_2^2 \|\mathbf{u} - \mathbf{v}\|_2^2, \quad (90)$$

$$\int_D |\nabla \theta(\mathbf{x} + \delta \boldsymbol{\eta}; \mathbf{u})|^4 d\mathbf{x} \leq 128\bar{J}_0^4 (C_{e_2}^2 + C_{e_1} C_{\omega_1}^2)^2 \|\mathbf{u}\|_2^4, \quad (91)$$

$$\int_D |\theta(\mathbf{x} + \delta \boldsymbol{\eta}; \mathbf{u} - \mathbf{v})|^2 |\nabla \theta(\mathbf{x} + \delta \boldsymbol{\eta}; \mathbf{v})|^4 d\mathbf{x} \leq 512\bar{J}_0^6 C_{e_1}^2 (C_{e_2}^2 + C_{e_1} C_{\omega_1}^2)^2 \|\mathbf{u} - \mathbf{v}\|_2^2 \|\mathbf{v}\|_2^4, \quad (92)$$

$$\int_D |\nabla^2 \theta(\mathbf{x} + \delta \boldsymbol{\eta}; \mathbf{u})|^2 d\mathbf{x} \leq 16\bar{J}_0^2 (1 + 2C_{\omega_1} + C_{\omega_2})^2 \|\mathbf{u}\|_2^2. \quad (93)$$

Here ∇ in all the equations above is with respect to \mathbf{x} . The constants C_{e_1}, C_{e_2} are the constants associated with the Sobolev embedding property of space $H^2(D; \mathbb{R}^d)$; see Eqs. 18 and 19.

Proof Using the notation given in Eq. 83, we write $\theta(\mathbf{x}; \mathbf{u})$ as

$$\theta(\mathbf{x}; \mathbf{u}) = \frac{1}{\omega_d} \int_{H_1(\mathbf{0})} \omega(\mathbf{x} + \epsilon \xi) J(|\xi|) \bar{\mathbf{u}}_\xi(\mathbf{x}) \cdot \mathbf{e}_\xi d\xi. \quad (94)$$

On noting that $|\bar{\mathbf{u}}_\xi(\mathbf{x})| \leq 2\|\mathbf{u}\|_\infty$ and $\|\mathbf{u}\|_\infty \leq C_{e_1} \|\mathbf{u}\|_2$, we easily see that

$$|\theta(\mathbf{x}; \mathbf{u})| \leq \bar{J}_0 2\|\mathbf{u}\|_\infty \leq 2C_{e_1} \bar{J}_0 \|\mathbf{u}\|_2. \quad (95)$$

In the rest of the proof, we will let $\mathbf{y} = \mathbf{x} + \delta\boldsymbol{\eta}$, where $0 \leq \delta \leq 2\epsilon$ and $\boldsymbol{\eta} \in H_1(\mathbf{0})$.

To show Eq. 88, we first introduce an important identity which will be used frequently. Let $p(\xi)$ be some function of ξ , and $\alpha, C \in \mathbb{R}$. Then,

$$\begin{aligned}
 & \left| \frac{C}{\omega_d} \int_{H_1(\mathbf{0})} \frac{J(|\xi|)}{|\xi|^\alpha} p(\xi) d\xi \right|^2 \\
 &= \left(\frac{C}{\omega_d} \right)^2 \int_{H_1(\mathbf{0})} \int_{H_1(\mathbf{0})} \frac{J(|\xi|)}{|\xi|^\alpha} \frac{J(|\eta|)}{|\eta|^\alpha} p(\xi) p(\eta) d\xi d\eta \\
 &\leq \left(\frac{C}{\omega_d} \right)^2 \int_{H_1(\mathbf{0})} \int_{H_1(\mathbf{0})} \frac{J(|\xi|)}{|\xi|^\alpha} \frac{J(|\eta|)}{|\eta|^\alpha} \frac{p(\xi)^2 + p(\eta)^2}{2} d\xi d\eta \\
 &= C^2 \frac{\bar{J}_\alpha}{\omega_d} \int_{H_1(\mathbf{0})} \frac{J(|\xi|)}{|\xi|^\alpha} p(\xi)^2 d\xi,
 \end{aligned} \tag{96}$$

where we used the inequality $ab \leq \frac{a^2}{2} + \frac{b^2}{2}$ in the first step, and definition of \bar{J}_α and symmetry of terms in the second step.

From the expression of $\theta(\mathbf{y}; \mathbf{u})$, we can show

$$\int_D |\theta(\mathbf{y}; \mathbf{u})|^2 dx \leq 4\bar{J}_0^2 \|\mathbf{u}\|^2 \leq 4\bar{J}_0^2 \|\mathbf{u}\|_2^2. \tag{97}$$

We now prove the bound Eq. 89. Taking the gradient of $\theta(\mathbf{y}; \mathbf{u})$, with respect to \mathbf{x} , noting that $\mathbf{y} = \mathbf{x} + \delta\boldsymbol{\eta}$, we get

$$\begin{aligned}
 \nabla \theta(\mathbf{y}; \mathbf{u}) &= \frac{1}{\omega_d} \int_{H_1(\mathbf{0})} J(|\xi|) \omega(\mathbf{y} + \epsilon\boldsymbol{\xi}) (\nabla \bar{\mathbf{u}}_\xi(\mathbf{y}))^\top \mathbf{e}_\xi d\xi \\
 &\quad + \frac{1}{\omega_d} \int_{H_1(\mathbf{0})} J(|\xi|) \nabla \omega(\mathbf{y} + \epsilon\boldsymbol{\xi}) \bar{\mathbf{u}}_\xi(\mathbf{y}) \cdot \mathbf{e}_\xi d\xi.
 \end{aligned} \tag{98}$$

We can show using the inequality Eq. 96 and the estimates $\int_D |\nabla \bar{\mathbf{u}}_\xi(\mathbf{y})|^2 dx \leq 4\|\nabla \mathbf{u}\|^2 \leq 4\|\mathbf{u}\|_2^2$, $|\nabla \omega(\mathbf{y} + \epsilon\boldsymbol{\xi})| \leq C_{\omega_1}$, $\int_D |\bar{\mathbf{u}}_\xi(\mathbf{y})|^2 dx \leq 4\|\mathbf{u}\|_2^2$, to conclude

$$\begin{aligned}
 \int_D |\nabla \theta(\mathbf{y}; \mathbf{u})|^2 dx &\leq \frac{2\bar{J}_0}{\omega_d} \int_{H_1(\mathbf{0})} J(|\xi|) 4\|\mathbf{u}\|_2^2 d\xi + \frac{2\bar{J}_0}{\omega_d} \int_{H_1(\mathbf{0})} J(|\xi|) 4C_{\omega_1}^2 \|\mathbf{u}\|_2^2 d\xi \\
 &= 8\bar{J}_0^2 (1 + C_{\omega_1}^2) \|\mathbf{u}\|_2^2 \leq 8\bar{J}_0^2 (1 + C_{\omega_1})^2 \|\mathbf{u}\|_2^2.
 \end{aligned} \tag{99}$$

We now show Eq. 90. We will use Eqs. 87 and 89, and proceed as follows:

$$\begin{aligned}
 & \int_D |\theta(\mathbf{y}; \mathbf{u} - \mathbf{v})|^2 |\nabla \theta(\mathbf{y}; \mathbf{v})|^2 dx \\
 &\leq \left(\sup_y |\theta(\mathbf{y}; \mathbf{u} - \mathbf{v})| \right)^2 \int_D |\nabla \theta(\mathbf{y}; \mathbf{v})|^2 dx \\
 &\leq 32\bar{J}_0^4 (1 + C_{\omega_1})^2 \|\mathbf{v}\|_2^2 \|\mathbf{u} - \mathbf{v}\|_2^2.
 \end{aligned} \tag{100}$$

To prove Eq. 91 we note expression of $\nabla\theta(\mathbf{y};\mathbf{u})$ in Eq. 98 and inequality $(a+b)^4 \leq 8a^4 + 8b^4$ and Eq. 96 to get

$$\begin{aligned} |\nabla\theta(\mathbf{y};\mathbf{u})|^4 &\leq \frac{64\bar{J}_0^3}{\omega_d} \int_{H_1(\mathbf{0})} J(|\xi|)(|\nabla\mathbf{u}(\mathbf{y} + \epsilon\xi)|^4 + |\nabla\mathbf{u}(\mathbf{y})|^4) d\xi \\ &\quad + \frac{64C_{\omega_1}^4 \bar{J}_0^3}{\omega_d} \int_{H_1(\mathbf{0})} J(|\xi|)(|\mathbf{u}(\mathbf{y} + \epsilon\xi)|^4 + |\mathbf{u}(\mathbf{y})|^4) d\xi. \end{aligned} \quad (101)$$

Application of Fubini's theorem gives

$$\begin{aligned} &\int_D |\nabla\theta(\mathbf{y};\mathbf{u})|^4 dx \\ &\leq \frac{64\bar{J}_0^3}{\omega_d} \int_{H_1(\mathbf{0})} J(|\xi|) \left(\int_D (|\nabla\mathbf{u}(\mathbf{y} + \epsilon\xi)|^4 + |\nabla\mathbf{u}(\mathbf{y})|^4) dx \right) d\xi \\ &\quad + \frac{64C_{\omega_1}^4 \bar{J}_0^3}{\omega_d} \int_{H_1(\mathbf{0})} J(|\xi|) \left(\int_D (|\mathbf{u}(\mathbf{y} + \epsilon\xi)|^4 + |\mathbf{u}(\mathbf{y})|^4) dx \right) d\xi \\ &\leq \frac{64\bar{J}_0^3}{\omega_d} \int_{H_1(\mathbf{0})} J(|\xi|) \left(2 \|\nabla\mathbf{u}\|_{L^4(D;\mathbb{R}^{d\times d})}^4 \right) d\xi \\ &\quad + \frac{64C_{\omega_1}^4 \bar{J}_0^3}{\omega_d} \int_{H_1(\mathbf{0})} J(|\xi|) \left(\|\mathbf{u}\|_\infty^2 \int_D (|\mathbf{u}(\mathbf{y} + \epsilon\xi)|^2 + |\mathbf{u}(\mathbf{y})|^2) dx \right) d\xi \\ &\leq 128\bar{J}_0^4 \|\nabla\mathbf{u}\|_{L^4(D;\mathbb{R}^{d\times d})}^4 + \frac{64C_{\omega_1}^4 \bar{J}_0^3}{\omega_d} \int_{H_1(\mathbf{0})} J(|\xi|) (\|\mathbf{u}\|_\infty^2 2 \|\mathbf{u}\|^2) d\xi \\ &\leq 128\bar{J}_0^4 \|\nabla\mathbf{u}\|_{L^4(D;\mathbb{R}^{d\times d})}^4 + 128C_{\omega_1}^4 \bar{J}_0^4 \|\mathbf{u}\|_\infty^2 \|\mathbf{u}\|^2. \end{aligned} \quad (102)$$

Using the Sobolev embedding property, $\|\mathbf{u}\|_\infty \leq C_{e_1} \|\mathbf{u}\|_2$ and $\|\nabla\mathbf{u}\|_{L^4} \leq C_{e_2} \|\mathbf{u}\|_2$, we obtain

$$\int_D |\nabla\theta(\mathbf{y};\mathbf{u})|^4 dx \leq 128\bar{J}_0^4 (C_{e_2}^4 + C_{e_1}^2 C_{\omega_1}^4) \|\mathbf{u}\|_2^4 \leq 128\bar{J}_0^4 (C_{e_2}^2 + C_{e_1} C_{\omega_1}^2)^2 \|\mathbf{u}\|_2^4. \quad (103)$$

The estimate Eq. 92 follows by combining estimates Eqs. 87 and 91. It now remains to show Eq. 93. From expression of $\nabla\theta(\mathbf{y};\mathbf{u})$ in Eq. 98, we have

$$\begin{aligned}
\nabla^2 \theta(\mathbf{y}; \mathbf{u}) &= \frac{1}{\omega_d} \int_{H_1(\mathbf{0})} J(|\xi|) \omega(\mathbf{y} + \epsilon \xi) \nabla^2 (\bar{\mathbf{u}}_\xi(\mathbf{y}) \cdot \mathbf{e}_\xi) d\xi \\
&\quad + \frac{1}{\omega_d} \int_{H_1(\mathbf{0})} J(|\xi|) ((\nabla(\bar{\mathbf{u}}_\xi(\mathbf{y}))^\top \mathbf{e}_\xi) \otimes \nabla \omega(\mathbf{y} + \epsilon \xi)) d\xi \\
&\quad + \frac{1}{\omega_d} \int_{H_1(\mathbf{0})} J(|\xi|) \nabla \omega(\mathbf{y} + \epsilon \xi) \otimes ((\nabla(\bar{\mathbf{u}}_\xi(\mathbf{y}))^\top \mathbf{e}_\xi) d\xi \\
&\quad + \frac{1}{\omega_d} \int_{H_1(\mathbf{0})} J(|\xi|) \nabla^2 \omega(\mathbf{y} + \epsilon \xi) \bar{\mathbf{u}}_\xi(\mathbf{y}) \cdot \mathbf{e}_\xi d\xi. \tag{104}
\end{aligned}$$

Using the equation above, we can show

$$\begin{aligned}
\int_D |\nabla^2 \theta(\mathbf{y}; \mathbf{u})|^2 d\mathbf{x} &\leq \frac{3\bar{J}_0}{\omega_d} \int_{H_1(\mathbf{0})} J(|\xi|) \left(\int_D |\nabla^2 \bar{\mathbf{u}}_\xi(\mathbf{y})|^2 d\mathbf{x} \right) d\xi \\
&\quad + \frac{12C_{\omega_1}^2 \bar{J}_0}{\omega_d} \int_{H_1(\mathbf{0})} J(|\xi|) \left(\int_D |\nabla \bar{\mathbf{u}}_\xi(\mathbf{y})|^2 d\mathbf{x} \right) d\xi \\
&\quad + \frac{3C_{\omega_2}^2 \bar{J}_0}{\omega_d} \int_{H_1(\mathbf{0})} J(|\xi|) \left(\int_D |\bar{\mathbf{u}}_\xi(\mathbf{y})|^2 d\mathbf{x} \right) d\xi. \tag{105}
\end{aligned}$$

The terms $|\bar{\mathbf{u}}_\xi(\mathbf{y})|^2$, $|\nabla \bar{\mathbf{u}}_\xi(\mathbf{y})|^2$, and $|\nabla^2 \bar{\mathbf{u}}_\xi(\mathbf{y})|^2$ are bounded by $2(|\mathbf{u}(\mathbf{y} + \epsilon \xi)|^2 + |\mathbf{u}(\mathbf{y})|^2)$, $2(|\nabla \mathbf{u}(\mathbf{y} + \epsilon \xi)|^2 + |\nabla \mathbf{u}(\mathbf{y})|^2)$, and $2(|\nabla^2 \mathbf{u}(\mathbf{y} + \epsilon \xi)|^2 + |\nabla^2 \mathbf{u}(\mathbf{y})|^2)$, respectively. Therefore, we have

$$\begin{aligned}
\int_D |\nabla^2 \theta(\mathbf{y}; \mathbf{u})|^2 d\mathbf{x} &\leq \left(3\bar{J}_0^2 + 12C_{\omega_1}^2 \bar{J}_0^2 + 3C_{\omega_2}^2 \bar{J}_0^2 \right) 4\|\mathbf{u}\|_2^2 \\
&\leq 16\bar{J}_0^2 (1 + C_{\omega_2} + 2C_{\omega_1})^2 \|\mathbf{u}\|_2^2, \tag{106}
\end{aligned}$$

and this completes the proof of lemma.

Estimating $\|\mathcal{L}_D^\epsilon(\mathbf{u}) - \mathcal{L}_D^\epsilon(\mathbf{v})\|$: We apply the notation described in Eq. 83, and write $\mathcal{L}_D^\epsilon(\mathbf{u})(\mathbf{x})$ as follows:

$$\mathcal{L}_D^\epsilon(\mathbf{u})(\mathbf{x}) = \frac{1}{\epsilon^2 \omega_D} \int_{H_1(\mathbf{0})} \omega_\xi(\mathbf{x}) J(|\xi|) [g'(\theta(\mathbf{x} + \epsilon \xi; \mathbf{u})) + g'(\theta(\mathbf{x}; \mathbf{u}))] \mathbf{e}_\xi d\xi. \tag{107}$$

Using the formula above and from the expression for θ , we can easily show

$$\|\mathcal{L}_D^\epsilon(\mathbf{u}) - \mathcal{L}_D^\epsilon(\mathbf{v})\| \leq \frac{L_1}{\epsilon^2} \|\mathbf{u} - \mathbf{v}\|_2, \tag{108}$$

where $L_1 = 4C_2^8 \bar{J}_0^2$.

Estimating $||\nabla \mathcal{L}_D^\epsilon(\mathbf{u}) - \nabla \mathcal{L}_D^\epsilon(\mathbf{v})||$: Taking the gradient of Eq. 107 gives

$$\begin{aligned}\nabla \mathcal{L}_D^\epsilon(\mathbf{u})(\mathbf{x}) &= \frac{1}{\epsilon^2 \omega_d} \int_{H_1(\mathbf{0})} J(|\xi|) \omega_\xi(\mathbf{x}) e_\xi \otimes [\nabla g'(\theta(\mathbf{x} + \epsilon \xi; \mathbf{u})) + \nabla g'(\theta(\mathbf{x}; \mathbf{u}))] d\xi \\ &\quad + \frac{1}{\epsilon^2 \omega_d} \int_{H_1(\mathbf{0})} J(|\xi|) e_\xi \otimes \nabla \omega_\xi(\mathbf{x}) [g'(\theta(\mathbf{x} + \epsilon \xi; \mathbf{u})) + g'(\theta(\mathbf{x}; \mathbf{u}))] d\xi \\ &=: G_1(\mathbf{u})(\mathbf{x}) + G_2(\mathbf{u})(\mathbf{x}),\end{aligned}\quad (109)$$

where we have denoted the first and second terms as $G_1(\mathbf{u})(\mathbf{x})$ and $G_2(\mathbf{u})(\mathbf{x})$ for convenience. On using the triangle inequality, we get

$$||\nabla \mathcal{L}_D^\epsilon(\mathbf{u}) - \nabla \mathcal{L}_D^\epsilon(\mathbf{v})|| \leq ||G_1(\mathbf{u}) - G_1(\mathbf{v})|| + ||G_2(\mathbf{u}) - G_2(\mathbf{v})||.$$

From the expression of $G_1(\mathbf{u})$, we have

$$\begin{aligned}|G_1(\mathbf{u})(\mathbf{x}) - G_1(\mathbf{v})(\mathbf{x})| &\leq \frac{1}{\epsilon^2 \omega_d} \int_{H_1(\mathbf{0})} J(|\xi|) (|\nabla g'(\theta(\mathbf{x} + \epsilon \xi; \mathbf{u})) - \nabla g'(\theta(\mathbf{x} + \epsilon \xi; \mathbf{v}))| \\ &\quad + |\nabla g'(\theta(\mathbf{x}; \mathbf{u})) - \nabla g'(\theta(\mathbf{x}; \mathbf{v}))|) d\xi.\end{aligned}$$

Let

$$p_1(\mathbf{y}) := |\nabla g'(\theta(\mathbf{y}; \mathbf{u})) - \nabla g'(\theta(\mathbf{y}; \mathbf{v}))| \quad (110)$$

and we get

$$||G_1(\mathbf{u}) - G_1(\mathbf{v})||^2 \leq \left(\frac{1}{\epsilon^2}\right)^2 \frac{2\bar{J}_0}{\omega_d} \int_{H_1(\mathbf{0})} J(|\xi|) \left(\int_D (p_1(\mathbf{x} + \epsilon \xi)^2 + p_1(\mathbf{x})^2) d\mathbf{x}\right) d\xi. \quad (111)$$

Note that

$$\nabla g'(\theta(\mathbf{x} + \epsilon \xi; \mathbf{u})) = g''(\theta(\mathbf{x} + \epsilon \xi; \mathbf{u})) \nabla \theta(\mathbf{x} + \epsilon \xi; \mathbf{u}).$$

Therefore, from Eq. 110,

$$\begin{aligned}p_1(\mathbf{y}) &= |g''(\theta(\mathbf{y}; \mathbf{u})) \nabla \theta(\mathbf{y}; \mathbf{u}) - g''(\theta(\mathbf{y}; \mathbf{v})) \nabla \theta(\mathbf{y}; \mathbf{v})| \\ &\leq C_2^g |\nabla \theta(\mathbf{y}; \mathbf{u}) - \nabla \theta(\mathbf{y}; \mathbf{v})| + C_3^g |\theta(\mathbf{y}; \mathbf{u}) - \theta(\mathbf{y}; \mathbf{v})| |\nabla \theta(\mathbf{y}; \mathbf{v})| \\ &= C_2^g |\nabla \theta(\mathbf{y}; \mathbf{u} - \mathbf{v})| + C_3^g |\theta(\mathbf{y}; \mathbf{u} - \mathbf{v})| |\nabla \theta(\mathbf{y}; \mathbf{v})|,\end{aligned}$$

where we have added and subtracted $g''(\theta(\mathbf{y}; \mathbf{u})) \nabla \theta(\mathbf{y}; \mathbf{v})$ and used the fact that $g''(r) \leq C_2^g$ and $|g''(r_1) - g''(r_2)| \leq C_3^g |r_1 - r_2|$. We use the estimate on p_1 and proceed as follows:

$$\begin{aligned}\int_D p_1(\mathbf{y})^2 d\mathbf{x} &\leq 2(C_2^g)^2 \int_D |\nabla \theta(\mathbf{y}; \mathbf{u} - \mathbf{v})|^2 d\mathbf{x} \\ &\quad + 2(C_3^g)^2 \int_D |\theta(\mathbf{y}; \mathbf{u} - \mathbf{v})|^2 |\nabla \theta(\mathbf{y}; \mathbf{v})|^2 d\mathbf{x},\end{aligned}$$

where we denote $\mathbf{x} + \epsilon \xi$ as \mathbf{y} . We apply inequality Eqs. 89 and 90 of Lemma 4 to obtain

$$\begin{aligned}\int_D p_1(\mathbf{y})^2 d\mathbf{x} &\leq 2(C_2^g)^2 8\bar{J}_0^2 (1 + C_{\omega_1})^2 ||\mathbf{u} - \mathbf{v}||_2^2 \\ &\quad + 2(C_3^g)^2 32\bar{J}_0^4 (1 + C_{\omega_1})^2 ||\mathbf{v}||_2^2 ||\mathbf{u} - \mathbf{v}||_2^2 \\ &\leq L_2 (1 + ||\mathbf{v}||_2)^2 ||\mathbf{u} - \mathbf{v}||_2^2,\end{aligned}$$

where we have grouped all the constant factors together and denote their product by L_2 . Substituting these estimates into Eq. 111 gives

$$\begin{aligned} ||G_1(\mathbf{u}) - G_1(\mathbf{v})||^2 &\leq \frac{4L_2\bar{J}_0^2}{\epsilon^4}(1 + ||\mathbf{v}||_2)^2 ||\mathbf{u} - \mathbf{v}||_2^2 \\ \Rightarrow ||G_1(\mathbf{u}) - G_1(\mathbf{v})|| &\leq \frac{L_3(1 + ||\mathbf{v}||_2)}{\epsilon^2} ||\mathbf{u} - \mathbf{v}||_2, \end{aligned} \quad (112)$$

where we have introduced the new constant L_3 .

The formula for $G_2(\mathbf{u})$ is similar to $\mathcal{L}_D^\epsilon(\mathbf{u})$ and, therefore, we have

$$||G_2(\mathbf{u}) - G_2(\mathbf{v})|| \leq \frac{C_{\omega_1}L_1}{\epsilon^2} ||\mathbf{u} - \mathbf{v}||_2.$$

Collecting results, we have shown

$$||\nabla \mathcal{L}_D^\epsilon(\mathbf{u}) - \nabla \mathcal{L}_D^\epsilon(\mathbf{v})|| \leq \frac{L_4(1 + ||\mathbf{v}||_2)}{\epsilon^2} ||\mathbf{u} - \mathbf{v}||_2, \quad (113)$$

where we have introduced new constant L_4 .

Estimating $||\nabla^2 \mathcal{L}_D^\epsilon(\mathbf{u}) - \nabla^2 \mathcal{L}_D^\epsilon(\mathbf{v})||$: Taking the gradient of Eq. 109, gives

$$\begin{aligned} \nabla^2 \mathcal{L}_D^\epsilon(\mathbf{u})(\mathbf{x}) &= \frac{1}{\epsilon^2 \omega_d} \int_{H_1(\mathbf{0})} \omega_\xi(\mathbf{x}) J(|\xi|) \mathbf{e}_\xi \otimes [\nabla^2 g'(\theta(\mathbf{x} + \epsilon\xi; \mathbf{u})) + \nabla^2 g'(\theta(\mathbf{x}; \mathbf{u}))] d\xi \\ &\quad + \frac{1}{\epsilon^2 \omega_d} \int_{H_1(\mathbf{0})} J(|\xi|) \mathbf{e}_\xi \otimes [\nabla g'(\theta(\mathbf{x} + \epsilon\xi; \mathbf{u})) + \nabla g'(\theta(\mathbf{x}; \mathbf{u}))] \otimes \nabla \omega_\xi(\mathbf{x}) d\xi \\ &\quad + \frac{1}{\epsilon^2 \omega_d} \int_{H_1(\mathbf{0})} J(|\xi|) \mathbf{e}_\xi \otimes \nabla \omega_\xi(\mathbf{x}) \otimes [\nabla g'(\theta(\mathbf{x} + \epsilon\xi; \mathbf{u})) + \nabla g'(\theta(\mathbf{x}; \mathbf{u}))] d\xi \\ &\quad + \frac{1}{\epsilon^2 \omega_d} \int_{H_1(\mathbf{0})} J(|\xi|) \mathbf{e}_\xi \otimes \nabla^2 \omega_\xi(\mathbf{x}) [g'(\theta(\mathbf{x} + \epsilon\xi; \mathbf{u})) + g'(\theta(\mathbf{x}; \mathbf{u}))] d\xi \\ &=: H_1(\mathbf{u})(\mathbf{x}) + H_2(\mathbf{u})(\mathbf{x}) + H_3(\mathbf{u})(\mathbf{x}) + H_4(\mathbf{u})(\mathbf{x}). \end{aligned} \quad (114)$$

It is easy to see that estimate on $||H_2(\mathbf{u}) - H_2(\mathbf{v})||$ and $||H_3(\mathbf{u}) - H_3(\mathbf{v})||$ is similar to the estimate for $||G_1(\mathbf{u}) - G_1(\mathbf{v})||$. Thus, from Eq. 112, we have

$$||H_2(\mathbf{u}) - H_2(\mathbf{v})|| + ||H_3(\mathbf{u}) - H_3(\mathbf{v})|| \leq \frac{2C_{\omega_1}L_3(1 + ||\mathbf{v}||_2)}{\epsilon^2} ||\mathbf{u} - \mathbf{v}||_2. \quad (115)$$

Also the estimate for $||H_4(\mathbf{u}) - H_4(\mathbf{v})||$ is similar to the estimate for $||G_2(\mathbf{u}) - G_2(\mathbf{v})||$ and we conclude

$$||H_4(\mathbf{u}) - H_4(\mathbf{v})|| \leq \frac{C_{\omega_2}L_1}{\epsilon^2} ||\mathbf{u} - \mathbf{v}||_2. \quad (116)$$

We now work on $||H_1(\mathbf{u}) - H_1(\mathbf{v})||$. From expression of $H_1(\mathbf{u})(\mathbf{x})$ in Eq. 114, we can easily get the following:

$$\begin{aligned} |H_1(\mathbf{u})(\mathbf{x}) - H_1(\mathbf{v})(\mathbf{x})| &\leq \frac{1}{\epsilon^2 \omega_d} \int_{H_1(\mathbf{0})} J(|\xi|) (|\nabla^2 g'(\theta(\mathbf{x} + \epsilon\xi; \mathbf{u})) - \nabla^2 g'(\theta(\mathbf{x} + \epsilon\xi; \mathbf{v}))| \\ &\quad + |\nabla^2 g'(\theta(\mathbf{x}; \mathbf{u})) - \nabla^2 g'(\theta(\mathbf{x}; \mathbf{v}))|) d\xi. \end{aligned} \quad (117)$$

Let $p_2(\mathbf{y})$, where $\mathbf{y} = \mathbf{x} + \epsilon \boldsymbol{\xi}$ and ∇ is with respect to \mathbf{x} , is given by

$$p_2(\mathbf{y}) := |\nabla^2 g'(\theta(\mathbf{y}; \mathbf{u})) - \nabla^2 g'(\theta(\mathbf{y}; \mathbf{v}))|. \quad (118)$$

We then have

$$||H_1(\mathbf{u}) - H_1(\mathbf{v})||^2 \leq \left(\frac{1}{\epsilon^2}\right)^2 \frac{2\bar{J}_0}{\omega_d} \int_{H_1(\mathbf{0})} J(|\boldsymbol{\xi}|) \left(\int_D (p_2(\mathbf{x} + \epsilon \boldsymbol{\xi})^2 + p_2(\mathbf{x})^2) d\mathbf{x} \right) d\boldsymbol{\xi}. \quad (119)$$

Note that

$$\nabla^2 g'(\theta(\mathbf{y}; \mathbf{u})) = g'''(\theta(\mathbf{y}; \mathbf{u})) \nabla \theta(\mathbf{y}; \mathbf{u}) \otimes \nabla \theta(\mathbf{y}; \mathbf{u}) + g''(\theta(\mathbf{y}; \mathbf{u})) \nabla^2 \theta(\mathbf{y}; \mathbf{u}).$$

We add and subtract terms to the equation above to get

$$\begin{aligned} & \nabla^2 g'(\theta(\mathbf{y}; \mathbf{u})) - \nabla^2 g'(\theta(\mathbf{y}; \mathbf{v})) \\ &= g'''(\theta(\mathbf{y}; \mathbf{u})) [\nabla \theta(\mathbf{y}; \mathbf{u}) \otimes \nabla \theta(\mathbf{y}; \mathbf{u}) - \nabla \theta(\mathbf{y}; \mathbf{v}) \otimes \nabla \theta(\mathbf{y}; \mathbf{v})] \\ &+ [g'''(\theta(\mathbf{y}; \mathbf{u})) - g'''(\theta(\mathbf{y}; \mathbf{v}))] \nabla \theta(\mathbf{y}; \mathbf{v}) \otimes \nabla \theta(\mathbf{y}; \mathbf{v}) \\ &+ g''(\theta(\mathbf{y}; \mathbf{u})) [\nabla^2 \theta(\mathbf{y}; \mathbf{u}) - \nabla^2 \theta(\mathbf{y}; \mathbf{v})] \\ &+ [g''(\theta(\mathbf{y}; \mathbf{u})) - g''(\theta(\mathbf{y}; \mathbf{v}))] \nabla^2 \theta(\mathbf{y}; \mathbf{v}). \end{aligned}$$

Using inequalities $|g''(r)| \leq C_2^g$, $|g'''(r)| \leq C_3^g$, $|g''(r_1) - g''(r_2)| \leq C_3^g |r_1 - r_2|$, $|g'''(r_1) - g'''(r_2)| \leq C_4^g |r_1 - r_2|$, and $|\mathbf{a} \otimes \mathbf{a} - \mathbf{c} \otimes \mathbf{c}| \leq (|\mathbf{a}| + |\mathbf{c}|) |\mathbf{a} - \mathbf{c}|$, and the fact that $\theta(\mathbf{y}; \mathbf{u}) - \theta(\mathbf{y}; \mathbf{v}) = \theta(\mathbf{y}; \mathbf{u} - \mathbf{v})$, we have

$$\begin{aligned} p_2(\mathbf{y}) &\leq C_3^g |\nabla \theta(\mathbf{y}; \mathbf{u})| |\nabla \theta(\mathbf{y}; \mathbf{u} - \mathbf{v})| + C_3^g |\nabla \theta(\mathbf{y}; \mathbf{v})| |\nabla \theta(\mathbf{y}; \mathbf{u} - \mathbf{v})| \\ &+ C_4^g |\theta(\mathbf{y}; \mathbf{u} - \mathbf{v})| |\nabla \theta(\mathbf{y}; \mathbf{v})|^2 \\ &+ C_2^g |\nabla^2 \theta(\mathbf{y}; \mathbf{u} - \mathbf{v})| + C_3^g |\theta(\mathbf{y}; \mathbf{u} - \mathbf{v})| |\nabla^2 \theta(\mathbf{y}; \mathbf{v})|. \end{aligned}$$

Taking the square of the above equation and using $\left(\sum_{i=1}^5 a_i\right)^2 \leq 5 \sum_{i=1}^5 a_i^2$ gives

$$\begin{aligned} \int_D p_2(\mathbf{y})^2 d\mathbf{x} &\leq 5(C_3^g)^2 \int_D |\nabla \theta(\mathbf{y}; \mathbf{u})|^2 |\nabla \theta(\mathbf{y}; \mathbf{u} - \mathbf{v})|^2 d\mathbf{x} \\ &+ 5(C_3^g)^2 \int_D |\nabla \theta(\mathbf{y}; \mathbf{v})|^2 |\nabla \theta(\mathbf{y}; \mathbf{u} - \mathbf{v})|^2 d\mathbf{x} \\ &+ 5(C_4^g)^2 \int_D |\theta(\mathbf{y}; \mathbf{u} - \mathbf{v})|^2 |\nabla \theta(\mathbf{y}; \mathbf{v})|^4 d\mathbf{x} \\ &+ 5(C_2^g)^2 \int_D |\nabla^2 \theta(\mathbf{y}; \mathbf{u} - \mathbf{v})|^2 d\mathbf{x} \\ &+ 5(C_3^g)^2 \int_D |\theta(\mathbf{y}; \mathbf{u} - \mathbf{v})|^2 |\nabla^2 \theta(\mathbf{y}; \mathbf{v})|^2 d\mathbf{x} \\ &=: I_1 + I_2 + I_3 + I_4 + I_5. \end{aligned}$$

We now estimate each term using Lemma 4 as follows. Applying the Hölder inequality and the inequality Eq. 91 of Lemma 4 we get

$$\begin{aligned} I_1 &\leq 5(C_3^g)^2 \left(\int_D |\nabla \theta(\mathbf{y}; \mathbf{u})|^4 d\mathbf{x} \right)^{1/2} \left(\int_D |\nabla \theta(\mathbf{y}; \mathbf{u} - \mathbf{v})|^4 d\mathbf{x} \right)^{1/2} \\ &\leq 640(C_3^g)^2 \bar{J}_0^4 (C_{e_2}^2 + C_{e_1} C_{\omega_1}^2)^2 \|\mathbf{u}\|_2^2 \|\mathbf{u} - \mathbf{v}\|_2^2. \end{aligned}$$

Similarly,

$$I_2 \leq 640(C_3^g)^2 \bar{J}_0^4 (C_{e_2}^2 + C_{e_1} C_{\omega_1}^2)^2 \|\mathbf{v}\|_2^2 \|\mathbf{u} - \mathbf{v}\|_2^2.$$

Using Eq. 92 of Lemma 4, we get

$$I_3 \leq 2560(C_4^g)^2 \bar{J}_0^6 (C_{e_2}^2 + C_{e_1} C_{\omega_1}^2)^2 \|\mathbf{v}\|_2^4 \|\mathbf{u} - \mathbf{v}\|_2^2.$$

For I_4 , we use the inequality Eq. 93 to get

$$I_4 \leq 80(C_2^g)^2 \bar{J}_0^2 (1 + 2C_{\omega_1} + C_{\omega_2})^2 \|\mathbf{u} - \mathbf{v}\|_2^2.$$

In I_5 , we use Eqs. 87 and 93 to get

$$I_5 \leq 320 \bar{J}_0^4 C_{e_1}^2 (1 + 2C_{\omega_1} + C_{\omega_2})^2 \|\mathbf{v}\|_2^2 \|\mathbf{u} - \mathbf{v}\|_2^2.$$

After collecting results, we can find a constant L_5 such that we have

$$\int_D p_2(\mathbf{y})^2 d\mathbf{x} \leq L_5^2 (1 + (\|\mathbf{u}\|_2 + \|\mathbf{v}\|_2) + (\|\mathbf{u}\|_2 + \|\mathbf{v}\|_2)^2)^2 \|\mathbf{u} - \mathbf{v}\|_2^2. \quad (120)$$

We substitute Eq. 120 into Eq. 119 to show

$$\begin{aligned} \|H_1(\mathbf{u}) - H_1(\mathbf{v})\|^2 &\leq \frac{4L_5^2 \bar{J}_0^2 (1 + (\|\mathbf{u}\|_2 + \|\mathbf{v}\|_2) + (\|\mathbf{u}\|_2 + \|\mathbf{v}\|_2)^2)^2}{\epsilon^4} \|\mathbf{u} - \mathbf{v}\|_2^2 \\ \Rightarrow \|H_1(\mathbf{u}) - H_1(\mathbf{v})\| &\leq \frac{L_6 (1 + (\|\mathbf{u}\|_2 + \|\mathbf{v}\|_2) + (\|\mathbf{u}\|_2 + \|\mathbf{v}\|_2)^2)}{\epsilon^2} \|\mathbf{u} - \mathbf{v}\|_2 \\ &\leq \frac{L_6 (1 + \|\mathbf{u}\|_2 + \|\mathbf{v}\|_2)^2}{\epsilon^2} \|\mathbf{u} - \mathbf{v}\|_2, \end{aligned} \quad (121)$$

where we have introduced the new constant L_6 .

We combine the estimates on H_1, H_2, H_3, H_4 , introducing a new constant L_7 , and get

$$\|\nabla^2 \mathcal{L}_D^\epsilon(\mathbf{u}) - \nabla^2 \mathcal{L}_D^\epsilon(\mathbf{v})\| \leq \frac{L_7 (1 + \|\mathbf{u}\|_2 + \|\mathbf{v}\|_2)^2}{\epsilon^2} \|\mathbf{u} - \mathbf{v}\|_2. \quad (122)$$

On adding the estimates, Eqs. 108, 113, 122, it is evident that the proof of Theorem 1 is complete.

6.2 Proof of Higher Temporal Regularity

In this section, we prove that the peridynamic evolutions have higher regularity in time for body forces that are differentiable in time. To see this we take the time derivative of Eq. 11 to get a second-order differential equation in time for $v = \dot{u}$ given by

$$\rho \partial_t^2 v(x, t) = Q(v(t); u(t))(x) + \dot{b}(x, t), \quad (123)$$

where $Q(v; u)$ is an operator that depends on the solution u of Eq. 11 and acts on v . It is given by

$$Q(v; u)(x) = Q_T(v; u)(x) + Q_D(v; u)(x), \quad \forall x \in D, \quad (124)$$

where

$$\begin{aligned} Q_T(v; u)(x) &= \frac{2}{\epsilon^d \omega_d} \int_{H_\epsilon(x)} \omega(x) \omega(y) \frac{J^\epsilon(|y - x|)}{\epsilon |y - x|} \\ &\quad \cdot \partial_{SS}^2 f(\sqrt{|y - x|} S(y, x, t; u)) S(y, x, t; v) e_{y-x} dy, \end{aligned} \quad (125)$$

and

$$\begin{aligned} Q_D(v; u)(x) &= \frac{1}{\epsilon^d \omega_d} \int_{H_\epsilon(x)} \omega(x) \omega(y) \frac{J^\epsilon(|y - x|)}{\epsilon^2} \\ &\quad \cdot [\partial_{\theta\theta}^2 g(\theta(y, t; u)) \theta(y, t; v) + \partial_{\theta\theta}^2 g(\theta(x, t; u)) \theta(x, t; v)] e_{y-x} dy. \end{aligned} \quad (126)$$

Clearly, for u fixed, the form $Q(v; u)$ acts linearly on v which implies that the equation for v is a linear nonlocal equation. The linearity of $Q(v; u)$ implies the Lipschitz continuity for $v \in W$ as stated below.

Theorem 7 (Lipschitz continuity of Q) *Let $u \in W$ be any given field. Then, for all $v, w \in W$, we have*

$$\|Q(v; u) - Q(w; u)\|_2 \leq \frac{L_8(1 + \|u\|_2)^2}{\epsilon^3} \|v - w\|_2, \quad (127)$$

where the constant L_8 does not depend on u, v, w . This gives for all $v \in W$ the upper bound,

$$\|Q(v; u)\|_2 \leq \frac{L_8(1 + \|u\|_2)^2}{\epsilon^3} \|v\|_2. \quad (128)$$

The proof follows the same steps used in the proof of Theorem 1.

If u is a peridynamic solution such that $u \in C^2(I_0; W)$, then we have for all $t \in I_0$, the inequality

$$\|Q(v; u(t))\|_2 \leq \frac{L_8(1 + \sup_{s \in I_0} \|u(s)\|_2)^2}{\epsilon^3} \|v\|_2. \quad (129)$$

Note that the Lipschitz continuity of $\dot{\mathbf{u}}(t)$ stated in Theorem 2 implies $\lim_{t \rightarrow 0^\pm} \partial_t^2 \mathbf{u}(\mathbf{x}, t) = \partial_t^2 \mathbf{u}(\mathbf{x}, 0)$. We now demonstrate that $\mathbf{v}(\mathbf{x}, t) = \partial_t \mathbf{u}(\mathbf{x}, t)$ is the unique solution of the following initial boundary value problem.

Theorem 8 (Initial value problem for $\mathbf{v}(\mathbf{x}, t)$) *Suppose the initial data and righthand side $\mathbf{b}(t)$ satisfy the hypothesis of Theorem 2 and we suppose further that $\dot{\mathbf{b}}(t)$ exists and is continuous in time for $t \in I_0$ and $\sup_{t \in I_0} \|\dot{\mathbf{b}}(t)\|_2 < \infty$. Then, $\mathbf{v}(\mathbf{x}, t)$ is the unique solution to the initial value problem $\mathbf{v}(\mathbf{x}, 0) = \mathbf{v}_0(\mathbf{x}), \partial_t \mathbf{v}(\mathbf{x}, 0) = \partial_t^2 \mathbf{u}(\mathbf{x}, 0),$*

$$\rho \partial_t^2 \mathbf{v}(\mathbf{x}, t) = Q(\mathbf{v}(t); \mathbf{u}(t))(\mathbf{x}) + \dot{\mathbf{b}}(\mathbf{x}, t), \quad t \in I_0, \mathbf{x} \in D, \quad (130)$$

$\mathbf{v} \in C^2(I_0; W)$ and

$$\|\partial_t^2 \mathbf{v}(\mathbf{x}, t)\|_2 \leq \|Q(\mathbf{v}(t); \mathbf{u}(t))(\mathbf{x})\|_2 + \|\dot{\mathbf{b}}(\mathbf{x}, t)\|_2. \quad (131)$$

Theorem 3 now follows immediately from Theorem 8 noting that $\partial_t \mathbf{u}(\mathbf{x}, t) = \mathbf{v}(\mathbf{x}, t)$ together with Eqs. 129 and 131. The proof of Theorem 8 follows from the Lipschitz continuity Eq. 127 and the Banach fixed point theorem as in [6].

7 Conclusions

In this article, we have provided a priori error estimates for finite element approximations to nonlocal state-based peridynamic fracture models. We have shown that the convergence rate applies even over time intervals for which the material is softening over parts of the computational domain. The results are established for two different classes of state-based peridynamic forces. The convergence rate of the approximation is of the form $C(\Delta t + h^2/\epsilon^2)$ where the constant C depends on ϵ and the H^2 norm of the solution and its time derivatives. For fixed Δt numerical simulations for Plexiglass show that the error decreases at the rate of h^2 at $40\ \mu\text{s}$ into the simulation. The simulations were carried out in parallel using 20 threads on a workstation with single Intel Xeon processor and with 32 GB of RAM. We anticipate similar convergence rates for longer times on bigger parallel machines.

We reiterate that the a priori error estimates account for the possible appearance of nonlinearity anywhere in the computational domain. On the other hand, numerical simulation and independent theoretical estimates show that the nonlinearity concentrates along “fat” cracks of finite length and width equal to ϵ ; see [25, 26]. Moreover, the remainder of the computational domain is seen to behave linearly and to leading order can be modeled as a linear elastic material up to an error proportional to ϵ ; see [Proposition 6, [22]]. Future work will use these observations to focus on the adaptive implementation and a-posteriori estimates.

Compliance with ethical standards

Funding This material is based upon work supported by the U. S. Army Research Laboratory and the U. S. Army Research Office under contract/Grant number W911NF1610456.

References

1. Agwai, A., Guven, I., Madenci, E.: Predicting crack propagation with peridynamics: a comparative study. *Int. J. Fract.* **171**(1), 65–78 (2011)
2. Aksoylu, B., Unlu, Z.: Conditioning analysis of nonlocal integral operators in fractional Sobolev spaces. *SIAM J. Numer. Anal.* **52**, 653–677 (2014)
3. Bobaru, F., Hu, W.: The meaning, selection, and use of the peridynamic horizon and its relation to crack branching in brittle materials. *Int. J. Fract.* **176**(2), 215–222 (2012)
4. Bobaru, F., Foster, J.T., Geubelle, P.H., Geubelle, P.H., Silling, S.A.: *Handbook of Peridynamic Modeling*. CRC, Boca Raton (2016)
5. Brenner, S., Scott, R.: *The Mathematical Theory of Finite Element Methods*, vol. 15, 3rd edn. Springer, Berlin (2007)
6. Brezis, H.: *Analyse Fonctionnelle, Théorie et Application*. Dunod, Paris (1983)
7. Chen, X., Gunzburger, M.: Continuous and discontinuous finite element methods for a peridynamics model of mechanics. *Comput. Methods Appl. Mech. Eng.* **200**(9), 1237–1250 (2011)
8. Demengel, F.: *Functional Spaces for the Theory of Elliptic Partial Differential Equations*. Universitext, 1st edn. Springer, London (2012)
9. Du, Q.: An invitation to nonlocal modeling, analysis and computation. In: *Proc. Int. Cong. of Math 2018*, Rio de Janeiro, vol. 3, pp. 3523–3552 (2018a)
10. Du, Q.: *Nonlocal Modeling, Analysis and Computation*. NSF-CBMS Monograph. SIAM, Philadelphia (2018b)
11. Du, Q., Gunzburger, M., Lehoucq, R., Zhou, K.: Analysis of the volume-constrained peridynamic navier equation of linear elasticity. *J. Elast.* **113**(2), 193–217 (2013a)
12. Du, Q., Ju, L., Tian, L., Zhou, K.: A posteriori error analysis of finite element method for linear nonlocal diffusion and peridynamic models. *Math. Comput.* **82**(284), 1889–1922 (2013b)
13. Du, Q., Tian, L., Zhao, X.: A convergent adaptive finite element algorithm for nonlocal diffusion and peridynamic models. *SIAM J. Numer. Anal.* **51**(2), 1211–1234 (2013c)
14. Emmrich, E., Lehoucq, R.B., Puhst, D.: *Peridynamics: a nonlocal continuum theory*. Meshfree Methods for Partial Differential Equations VI, pp. 45–65. Springer, Berlin (2013)
15. Foster, J.T., Silling, S.A., Chen, W.: An energy based failure criterion for use with peridynamic states. *Int. J. Multiscale Comput. Eng.* **9**(6), 675–688 (2011)
16. Gerstle, W., Sau, N., Silling, S.: Peridynamic modeling of concrete structures. *Nuclear Eng. Des.* **237**(12), 1250–1258 (2007)
17. Ghajari, M., Iannucci, L., Curtis, P.: A peridynamic material model for the analysis of dynamic crack propagation in orthotropic media. *Comput. Methods Appl. Mech. Eng.* **276**, 431–452 (2014)
18. Guan, Q., Gunzburger, M.: Stability and accuracy of time-stepping schemes and dispersion relations for a nonlocal wave equation. *Numer. Methods Part. Differ. Equ.* **31**(2), 500–516 (2015)
19. Ha, Y.D., Bobaru, F.: Studies of dynamic crack propagation and crack branching with peridynamics. *Int. J. Fract.* **162**(1/2), 229–244 (2010)
20. Jha, P. K., Lipton, R.: Finite element approximation of nonlinear nonlocal models (2017). arXiv preprint arXiv:1710.07661
21. Jha, P.K., Lipton, R.: Numerical analysis of nonlocal fracture models in Hölder space. *SIAM J. Numer. Anal.* **56**, 906–941 (2018a)
22. Jha, P.K., Lipton, R.: Numerical convergence of nonlinear nonlocal continuum models to local elastodynamics. *Int. J. Numer. Methods Eng.* **114**(13), 1389–1410 (2018b)
23. Jha, P. K., Lipton, R.: Small horizon limit of state based peridynamic models. In preparation (2019)
24. Karaa, S.: Stability and convergence of fully discrete finite element schemes for the acoustic wave equation. *J. Appl. Math. Comput.* **40**(1/2), 659–682 (2012)
25. Lipton, R.: Dynamic brittle fracture as a small horizon limit of peridynamics. *J. Elast.* **117**, 21–50 (2014)
26. Lipton, R.: Cohesive dynamics and brittle fracture. *J. Elast.* **124**(2), 143–191 (2016)
27. Lipton, R., Silling, S., Lehoucq, R.: Complex fracture nucleation and evolution with nonlocal elastodynamics (2016). arXiv preprint arXiv:1602.00247
28. Lipton, R., Said, E., Jha, P.: Free damage propagation with memory. *J. Elast.* **133**(2), 129–153 (2018a)
29. Lipton, R., Said, E., Jha, P.K.: Dynamic brittle fracture from nonlocal double-well potentials: a state-based model. In: *Handbook of Nonlocal Continuum Mechanics for Materials and Structures*, pp. 1–27 (2018b)
30. Littlewood, D. J.: Simulation of dynamic fracture using peridynamics, finite element modeling, and contact. In: *Proceedings of the ASME 2010 International Mechanical Engineering Congress and Exposition (IMECE)* (2010)

31. Macek, R.W., Silling, S.A.: Peridynamics via finite element analysis. *Finite Elem. Anal. Des.* **43**(15), 1169–1178 (2007)
32. Mengesha, T., Du, Q.: On the variational limit of a class of nonlocal functionals related to peridynamics. *Nonlinearity* **28**(11), 3999 (2015)
33. Ren, B., Wu, C., Askari, E.: A 3d discontinuous galerkin finite element method with the bond-based peridynamics model for dynamic brittle failure analysis. *Int. J. Impact Eng.* **99**, 14–25 (2017)
34. Silling, S.A.: Reformulation of elasticity theory for discontinuities and long-range forces. *J. Mech. Phys. Solids* **48**(1), 175–209 (2000)
35. Silling, S.A., Bobaru, F.: Peridynamic modeling of membranes and fibers. *Int. J. Non-Linear Mech.* **40**(2), 395–409 (2005)
36. Silling, S.A., Lehoucq, R.B.: Convergence of peridynamics to classical elasticity theory. *J. Elast.* **93**(1), 13–37 (2008)
37. Silling, S.A., Epton, M., Weckner, O., Xu, J., Askari, E.: Peridynamic states and constitutive modeling. *J. Elast.* **88**(2), 151–184 (2007)
38. Silling, S., Weckner, O., Askari, E., Bobaru, F.: Crack nucleation in a peridynamic solid. *Int. J. Fract.* **162**(1/2), 219–227 (2010)
39. Tian, X., Du, Q.: Asymptotically compatible schemes and applications to robust discretization of non-local models. *SIAM J. Numer. Anal.* **52**, 1641–1665 (2014)
40. Weckner, O., Abeyaratne, R.: The effect of long-range forces on the dynamics of a bar. *J. Mech. Phys. Solids* **53**(3), 705–728 (2005)